# The transition zone as a host for recycled volatiles: evidence from nitrogen and carbon isotopes in ultra-deep diamonds from Monastery and Jagersfontein (South Africa)

M. Palot[a*], D. G. Pearson[a], T. Stachel[a], R.A. Stern[a,b], A. Le Pioufle[a], J.J. Gurney[c] & J.W. Harris[d]

*corresponding author: mederic.palot@gmail.com now at Laboratoire Magmas et Volcans, Université Jean Monnet, Saint-Etienne, France.

[a] Department of Earth and Atmospheric Sciences, University of Alberta, Edmonton, Canada.

[b] Canadian Centre for Isotopic Microanalysis, University of Alberta, Edmonton, Canada.

[c] Department of Geological Sciences, University of Cape Town, Rondebosch, Republic of South Africa.

[d] School of Geographical and Earth Sciences, University of Glasgow, Scotland, United Kingdom.

## Abstract

Sublithospheric (ultra-deep) diamonds provide a unique window into the deepest parts of Earth's mantle, which otherwise remain inaccessible. Here, we report the first combined C- and N- isotopic data for diamonds from the Monastery and Jagersfontein kimberlites that sample the deep asthenosphere and transition zone beneath the Kaapvaal Craton, in the mid Cretaceous, to investigate the nature of mantle fluids at these depths and the constraints they provide on the deep volatile cycle.

Both diamond suites exhibit very light $\delta^{13}C$ values (down to -26‰) and heavy $\delta^{15}N$ (up to +10.3‰), with nitrogen abundances generally below 70 at.ppm but varying up to very high concentrations (2520 at.ppm) in rare cases. Combined, these signatures are consistent with derivation from subducted crustal materials. Both suites exhibit variable nitrogen aggregation states from 25 to 100 % B defects. Internal growth structures, revealed in cathodoluminescence

(CL) images, vary from faintly layered, through distinct cores to concentric growth patterns with intermittent evidence for dissolution and regular octahedral growth layers in places.

Modelling the internal co-variations in $\delta^{13}C$-$\delta^{15}N$-N revealed that diamonds grew from diverse C-H-O-N fluids involving both oxidised and reduced carbon species. The diversity of the modelled diamond-forming fluids highlights the complexity of the volatile sources and the likely heterogeneity of the deep asthenosphere and transition zone. We propose that the Monastery and Jagersfontein diamonds form in subducted slabs, where carbon is converted into either oxidised or reduced species during fluid-aided dissolution of subducted carbon before being re-precipitated as diamond. The common occurrence of recycled C and N isotopic signatures in super-deep diamonds world-wide indicates that a significant amount of carbon and nitrogen is recycled back to the deep asthenosphere and transition zone via subducting slabs, and that the transition zone may be dominated by recycled C and N.

**Keywords**

Monastery and Jagersfontein diamonds, ultra-deep diamonds, transition zone, carbon and nitrogen, subduction, oxidised and reduced fluids.

## 1. Introduction

Exchange of volatiles such as carbon and nitrogen between the Earth's interior and the surface is key to understanding mantle-surface interactions over geological time (Dasgupta and Hirschmann, 2010, Cartigny and Marty, 2013, Barry and Hilton, 2016). Carbon and nitrogen are ubiquitous amongst Earth's volatile components and their distinct isotopic compositions in different major reservoirs make them powerful tracers of volatile recycling in the deep solid Earth (Walter et al., 2011, Cartigny and Marty, 2013, Busigny and Bebout, 2013). Numerous

studies provide clear evidence for recycling of crustal carbon and nitrogen into the lithospheric mantle (Dasgupta et al., 2004, Halama et al., 2010, Busigny and Bebout, 2013, Mikhail et al., 2013, Smart et al., 2016), but little is known about the transport of C and N and their storage in the deeper, sublithospheric mantle due to the scarcity of direct samples from below 250 km depth. Diamond is a direct probe of this deeper segment of the Earth owing to its physical robustness and chemical inertness (Stachel et al., 2002, Stachel et al., 2005, 2009; Tappert et al., 2005a, Bulanova et al., 2010, Walter et al., 2011, Palot et al., 2012, 2014, 2016, Harte and Hudson, 2013, Kaminsky and Wirth, 2013, Burnham et al., 2015, 2016, Thomson et al., 2016a and b). Mineral inclusions in diamond indicate that the majority of diamonds formed in the lithospheric mantle, at depths of 150-200 km (see Stachel and Harris 2008, Shirey et al., 2013 for reviews). Very rare inclusions, in so-called ultra-deep diamonds, derive from greater depths within the transition zone (410-660 km) and the lower mantle (>660 km; see Stachel et al., 2005, Kaminsky, 2012 and Harte and Hudson, 2013 for reviews). Diamond, therefore, represents a unique opportunity to examine volatile migration within the deep asthenosphere and mantle transition zone that are otherwise inaccessible for geological sampling.

It is now well established that the vast majority of diamonds form by metasomatic fluid infiltration processes (Schrauder and Navon, 1993, Klein-BenDavid et al., 1994, Schulze et al. 1996, Taylor et al., 1996, Sobolev et al., 1998, Stachel et al., 2004), through redox reactions involving C-H-O-N-S fluids (Haggerty, 1986). This process is best reflected by core-to-rim variations of the C and N-isotopic composition within single diamonds because the progress of isotopic fractionation is a function of carbon and nitrogen speciation of the fluid. Spatially resolved accurate and precise in-situ analysis of both C and N isotopes in diamonds has only recently become accessible by secondary ion mass spectrometry (SIMS; Bulanova et al., 2002, Zedgenizov et al., 2014, Stern et al., 2014, Petts et al., 2016). This approach provides new

constraints on the origin and nature of diamond-forming fluids. So far, only "ultra-deep" diamonds from Kankan have been investigated in this way (Palot et al., 2014). There is hence a pressing need for additional studies on ultra-deep diamonds from other localities to better understand what these special samples have to offer in constraining the nature of C and N fluxing into the Earth's transition zone and lower mantle.

In this study, we present the first combined C and N-isotopic data for Monastery and Jagersfontein sublithospheric diamonds. We conducted infrared spectroscopy (FTIR), cathodoluminescence (CL) and in situ $\delta^{13}C$-$\delta^{15}N$-N analysis using SIMS on 15 ultra-deep diamonds from these two localities. All the samples contained majoritic garnet inclusions that allow their depth of origin to be constrained (Tappert et al., 2005a, b, Moore and Gurney, 1985; Moore et al., 1991). For our set of Jagersfontein diamonds, Tappert et al. (2005a, 2005b) analysed bulk $\delta^{13}C$ and Ickert et al. (2015) measured the oxygen isotope composition of some of the majorite inclusions.

## 2. Sample description

### 2.1 Monastery

The Monastery kimberlite erupted through the SE margin of the Kaapvaal Craton at ~ 90 Ma (Davis et al., 1980). Monastery diamonds are renowned for providing the first majoritic garnet inclusions, recognized by an excess of Si over the 3 available tetrahedral sites per formula unit (on the basis of 12 oxygens) (Moore and Gurney, 1985; Moore et al., 1991). Assuming inclusions are syngenetic, the majorites place diamond formation within the asthenosphere/transition zone at depths greater than 250 km (Moore & Gurney, 1985; Deines et al., 1991; Tappert et al., 2005a, 2005b), where pyroxene dissolution in garnet becomes significant (Irifune, 1987). Major and trace element analyses (Moore et al., 1991) show that these samples

are all eclogitic in composition. Using the majorite barometer for eclogitic compositions of Wijbrans et al. (2016) which is based on Si, Na and Ca content of the inclusion, led to estimates from 360 and 370 km depth for the four Monastery diamonds studied here (A4-03, B9-07, B9-15, B9-17) (Table 1; Fig. 1).

Diamond samples are ~600µm to ~1.4mm fragments of the original stones. Internal growth structures, revealed in CL (Fig. 2 and Appendix A), vary from faintly layered (A4-03, B9-17), through distinct core (B9-15) (Appendix A) to concentric growth patterns with intermittent evidence for dissolution and regular octahedral growth layers in places (B9-07; Fig. 2).

### 2.2 Jagersfontein

The 86 Ma old Jagersfontein kimberlite also erupted through the southern margin of the Kaapvaal Craton and is another kimberlite renowned for the presence of rare diamonds containing majoritic garnet inclusions (Deines et al., 1991; Stachel et al., 2005). The suite of majoritic garnet -bearing diamonds (11 samples) studied here was previously analysed for the major and trace element composition of their inclusions and bulk $\delta^{13}C$ of the host diamonds (Tappert et al., 2005a, 2005b). The sample suite contains garnets with an excess of Si cations ranging from 3.05 to 3.54 (Tappert et al., 2005a, 2005b). The depth of trapping of these inclusions through their host diamonds is estimated to have occurred between 240 and 410 km (Table 1; Fig. 1). As with the Monastery suite, all majorite inclusions in the diamonds studied here belong to the eclogitic parageneses, with <1 wt% $Cr_2O_3$ (Schulze, 2003), with the exception of sample JF43, whose garnet composition is websteritic (i.e. transitional between the eclogitic and peridotitic parageneses; Gurney et al., 1984).

All samples are < 1mm fragments of previously octahedral, dodecahedral or irregular diamonds (Tappert et al., 2005b). Despite the loss of their original shape, cathodoluminescence

images (Fig. 2 and Appendices B1-B3) exhibit internal growth/dissolution features that help constrain diamond structure and growth direction. Samples JF01, JF09, JF22, JF37, JF39, JF43, JF55 and JF58 exhibit faintly layered structures, while JF42, JF44 and JF50 present concentric growth patterns with intermittent evidence for dissolution (Appendices B1-B3).

## 3. Analytical methods

Diamonds were analysed for nitrogen content and nitrogen aggregation state in the De Beers Laboratory for Diamond Research at the University of Alberta, using a Thermo Nicolet Nexus 470 FT-IR Spectrometer fitted with a Continuum infrared microscope. The system was continuously purged with a dry nitrogen-oxygen mix. Spectra were acquired from 650-4000$cm^{-1}$ in transmission mode for 200 s with a resolution of 4 $cm^{-1}$ and an aperture size of 100 μm. Nitrogen concentrations and aggregation states were calculated after spectral decomposition using the Excel program CAXBD97, developed by David Fisher (De Beers Technologies UK). The absorption coefficients used for the A- and B-centers at 1282$cm^{-1}$ were 16.5 and 79.4 at.ppm/cm (Boyd et al., 1994, 1995), respectively. Detection limits and uncertainties typically range from 5 to 15 at. ppm and about 10% respectively. The uncertainty of the aggregation state of nitrogen is estimated to be better than ±5% (2σ).

Isotope data were determined by multicollector-secondary ion mass spectrometry (MC-SIMS, Cameca IMS 1280) at the Canadian Centre for Isotopic Microanalysis (CCIM), using methods and reference materials described by Stern et al. (2014). A tightly packed array of 16 diamonds was cast in epoxy, then ground and polished to reveal partial sections in random crystallographic orientation. Scanning electron microscopy (SEM) was conducted at 15 kV with a

Zeiss EVO MA15 equipped with a high sensitivity broadband cathodoluminescence detector (ETP Semra Pty Ltd). Subsequently, the epoxy mount was trimmed to create a 5 x 5 mm block. The diamond block was pressed into indium along with reference materials (RMs) S0011Cd diamond and a vitreous carbon RM to form mount M1148 used for C-isotope analyses. A second mount (M1192) containing the diamond block and RMs S0011Cd diamond and S0270 diamond was prepared for the purpose of N-isotope analysis. Mounts were initially coated with 7 nm of Au for cathodoluminescence imaging by SEM, and increased to 30 nm for SIMS analysis.

Diamonds were sputtered with a ~15 x 20 μm probe of $Cs^+$ primary ions of operating at 3.0 – 5.5 nA and 20 keV. Analyses of C-isotopes was followed by N abundance measurements in the same spot location, and then followed by N-isotopes from a closely-adjacent location in the same CL zone. Analyses involved simultaneous detection of pairs of negative secondary ions ($^{13}C/^{12}C^-$, $^{26}[^{14}N^{12}N]^-/^{24}[^{12}C^{12}C]^-$, $^{27}[^{15}N^{12}C]^-/^{26}[^{14}N^{12}C]^-$) at high mass resolution to resolve spectral interferences. C-isotope analyses utilized dual Faraday cups, N-isotopes utilized an electron multiplier–Faraday combination, and N-abundances utilized both depending on concentration. C-isotopic analyses of unknowns were referenced to interspersed analyses of S0011Cd diamond ($\delta^{13}C_{VPDB}$ = -22.58 ±0.10‰) and N-isotopes referenced to S0270 diamond ($\delta^{15}N_{AIR}$ = -0.4 ±0.5‰; Stern et al., 2014). Reported uncertainties in $\delta^{13}C_{VPDB}$ and $\delta^{15}N_{Air}$ include those related to instrumental mass fractionation and repeatability of reference materials; the absolute uncertainties in the reference materials listed above are not included. N-abundances (atomic fractions, parts per million) are referenced to diamond RMs analyzed by infrared spectroscopy and have an overall uncertainty of ±10%.

## 4. Results

### 4.1 Nitrogen abundance and aggregation state by FTIR

All Monastery diamonds are of the N-bearing Type I variety, with widely varying nitrogen contents and aggregation states. Mon B9-07 is a fully aggregated Type IaB diamond with 700 at.ppm N (Fig. 3), one of the highest N-abundances recorded in ultra-deep diamonds worldwide. Mon B9-15 is also a Type IaB diamond (91%), but with nitrogen contents as low as 20 at.ppm across the sample (Fig. 3). The other two specimens, Mon B9-17 and Mon A4-03 are Type IaAB (65% of B defects) and IaB (92%) with moderate nitrogen abundances of 50 and 40 at.ppm, respectively (Fig. 3).

The Jagersfontein sublithospheric diamonds exhibit much lower N abundances, <60 at.ppm (Tappert al., 2005a), compared to the Monastery diamonds. Only six of the eleven diamonds in this suite have detectable nitrogen (Fig. 3) and they exhibit variable nitrogen aggregation states (35-100 % B defect) (Fig. 3).

Average mantle residence temperatures ($T_{N\text{-}aggregation}$) have been calculated using a second order kinetic law linking the nitrogen concentration, the aggregation state of nitrogen in diamond and its residence time in the mantle (Chrenko et al., 1977). We assumed a short residence time of about 100 Ma (Tappert et al., 2005b) based on the occurrence of unexsolved majorite inclusions. Long-time storage and re-equilibration in the sub-continental lithospheric mantle would result in the exsolution of the pyroxene component in the majorite inclusion (Harte and Cayzer, 2007). Tappert et al. (2005) linked the genesis of these diamonds to the formation of the Cape Fold Belt ~200 Ma ago. Diamond exhumation occurs at the time of the kimberlite emplacement (86 Ma for Jagersfontein), leaving a ~100 Ma window for mantle residence.Calculated $T_{N\text{-}aggregation}$ range from 1280 to 1480°C, which is systematically lower than the majorite component-derived pressure and projected temperatures ($T_{inclusion}$) (Table 1).

### 4.2 Carbon isotopes composition and nitrogen abundances by SIMS

One to three profiles were analysed across each diamond in order to study the spatial variation of $\delta^{13}C$ and N-abundance in individual samples (Fig. 2; Appendices A, B1-B3, C and D1-D3; Tables 2 and 3).

#### 4.2.1 Monastery diamonds

Monastery diamonds exhibit strongly negative $\delta^{13}C$ compositions from -14.3‰ to -18.7‰ (Table 2, Appendix C). Most Monastery diamonds show only minor variability in $\delta^{13}C$ along profiles (<2‰ internal variation), except for Mon A4-03, which varies by 3.8‰ (Table 2, Appendix C). SIMS nitrogen abundances of Monastery diamonds are <70 at.ppm, except for Mon B9-07, which has exceptionally high N-abundances up to 2520 at.ppm (Table 2, Appendix C). This sample exhibits a weak zonation in $\delta^{13}C$ from -15.8 to -15.0‰, with a general increase of $\delta^{13}C$ values from core to rim (Fig. 4, Appendixes A and C). Nitrogen contents decrease from core to rim and are negatively correlated with the $\delta^{13}C$ values (Fig. 4). Mon B9-15 is isotopically homogeneous ($\delta^{13}C$ = -18.2 to -18.7‰) with Mon B9-17 being relatively so (-15.6 to -17.4) with no obvious core to rim zonations (Appendixes A and C). Both samples have N contents < 40 at.ppm with slight variation along profiles (Appendixes A and C). The $\delta^{13}C$ values of Mon A4-03 decrease from -14.3‰ (core) to -18.1‰ (rim) together with increasing N-abundance (2 to 65 at.ppm ; Fig. 6, Appendixes A and C).

#### 4.2.2 Jagersfontein diamonds

The $\delta^{13}C$ values of Jagersfontein diamonds range from -15.9‰ to -25.7‰ (Table 3), which despite the vast difference in sampling scale is in close agreement with the bulk analyses of Tappert et al. (2005a, b; $\delta^{13}C$ = -17.0‰ to –24.0‰). While some of the diamonds are relatively homogeneous in $\delta^{13}C$ (JF22, JF44, JF55), others show significant (>2‰) internal

variations (JF01, JF09, JF37, JF39, JF42, JF43, JF50, JF58), with a maximum variation of 5.9‰ (JF42) (Table 3, Appendixes D1-D3). Nitrogen concentrations also vary, although most of the values are below 70 at.ppm, with a few exceptions (JF39, JF50, JF55) (Table 3). Nitrogen abundances display a maximum of 308 at. ppm for JF39 (Table 3). Diamonds JF01, JF37 and JF43 present distinct core ($\delta^{13}C$ ~ -17‰, -22‰ and -23‰, respectively) and rim carbon isotope compositions (~ -21‰, -20‰ and -21‰, respectively) without any apparent correlation with nitrogen abundances (Appendices B1, B2, C1 and C2). Diamonds JF09, JF44 and JF50 exhibit core to rim trends with increasing $\delta^{13}C$ values and decreasing N-contents (Fig. 5 and 7, Appendixes B1, B2,D1-D3). Diamond JF58 shows clear variations from inner to outer zones with a decrease of $\delta^{13}C$ together with an increase in N concentration (Fig. 6, Appendices B3 and D3). All other samples exhibit either very slight or no clear $\delta^{13}C$ and N-abundance variations along transects (Appendixes B1-B3, D1-D3).

The carbon isotopic compositions of both suites of diamonds are significantly more negative than the typical current convective mantle (Cartigny et al., 2014, their Fig. 8).

### 4.3 Nitrogen isotopes

The spatial variability in nitrogen isotope composition ($\delta^{15}N$) was determined only for the diamonds with the highest nitrogen abundances (>80 at.ppm; Mon B9-07, JF39, JF50 and JF55, Appendix Tables 2 and 3).

#### 4.3.1 Monastery diamonds

High nitrogen concentrations in Mon B9-07 allowed multiple analyses of $\delta^{15}N$ across this diamond (Table 1). Three detailed profiles were obtained (Appendix E). The $\delta^{15}N$ values are all positive, varying significantly in all transects from, +3.8‰ to +10.3‰ (total variation of 6.5‰).

There is a negative correlation between increasing $\delta^{15}N$ and decreasing [N], which approximately corresponds to a core-rim trend (Fig. 4, Appendixes A and E). Because of the limited variations in $\delta^{13}C$ (~ 1‰), no clear trends with $\delta^{15}N$ could be determined outside of analytical uncertainty (Fig. 4). The precision of the nitrogen isotope measurements (typically < 1.5 ‰) allows us to clearly resolve that these compositions are significantly more positive than the current estimate for the convective mantle compositional range (Cartigny et al., 2014, Fig. 8).

#### 4.3.2 Jagersfontein diamonds

The low N abundances in the Jagersfontein samples made precise determination of their N isotopic compositions challenging and only few determinations were performed. Four N isotope analyses were obtained on diamond JF50 (Table 3). The variations in $\delta^{15}N$ are small, with relatively large uncertainties that are dictated by counting statistics due to the low [N] (-0.8±2.8‰ to +1.1±3.1‰). Nonetheless, the measurements are sufficiently precise to conclude that the N isotopic compositions are slightly $^{15}N$-enriched, at the upper end of the "mantle range" (Fig. 8). Because of the limited precision and apparent variations in $\delta^{15}N$, no clear trends with [N] and $\delta^{13}C$ could be determined outside of analytical uncertainty (Fig. 7). Only one analysis of $\delta^{15}N$ has been performed for JF55 ($\delta^{15}N$ = +7.1 ±1.6‰) and two for JF39 ($\delta^{15}N$ = +6.7 ±1.7‰ and +6.2 ±2.4‰; Table 3). The positive $\delta^{15}N$ values for both diamonds are significantly higher than typical mantle values (Fig. 8).

## 5. Discussion

### 5.1 Diamond growth associated with pulses of fluids

Solid state growth resulting from a direct conversion of graphite into diamond in a subduction environment setting was suggested as the main diamond genesis mechanism for the

Jagersfontein ultra-deep diamonds (Tappert et al., 2005a). This hypothesis is not supported by the observations detailed below. Instead, the precipitation of ultra-deep diamonds associated with the percolation/pulses of fluid(s) (i.e. metasomatism) is preferred (Stachel et al., 2002, Palot et al., 2014, 2016 Pearson et al., 2014, Thomson et al., 2014, 2016, Zedgenizov et al. 2014, Burnham et al., 2015, 2016).

Although the study of only fragments makes the interpretation of the diamond growth histories difficult, the CL images still permit some inferences to be made. Amongst the Monastery diamonds, the CL images of Mon B9-15 and B9-17 do not reveal any clear growth history, whereas Mon A4-03 possibly exhibits multiple growth episodes (Appendix A). Mon B9-07 displays regular growth layers (Fig. 2) and the growth of this diamond is interrupted by several dissolution episodes. Amongst the Jagersfontein diamonds, all but JF22 and JF58 show a clear separation into core and rim zones (Appendixes B1-B3).

From the textural evidence noted above, most of the studied diamonds document episodic growth, identified by sharp boundaries between CL "layers" (Appendixes A, B1-B2), sometimes with intermittent periods of resorption (visible truncations of growth layers). These features are characteristic of diamond growth from intermittent fluid/melt pulses. The distinct dark to bright CL responses may thus be interpreted in terms of diamond growth from fluid pulses with varying composition or under variable pressure-temperature conditions; episodes of dissolution correspond to the intermittent passage of fluids that are undersaturated in carbon or relatively oxidizing. In diamonds JF39, JF42 and JF43, these CL features are associated with sharp changes in isotopic composition and nitrogen abundance (Appendix D2), suggesting that each zone represents a discrete phase of diamond growth during distinct pulses of fluids. In contrast, smooth co-variations are often interpreted as diamond growth from an evolving fluid (Cartigny et al., 2014 for review, see section 5.3 below).

### 5.2 The source of fluids forming ultra-deep diamonds

The very negative $\delta^{13}C$ values and positive $\delta^{15}N$ values for the ultra-deep diamonds studied here depart significantly from typical mantle values (Fig. 8). In diamonds where core-rim relationships can be established from growth textures, growth already begins from fluids with such distinctive isotopic compositions. The consistency of this observation can only be explained by diamond formation from fluids that ultimately derive from surficial material subducted into the deep asthenosphere or transition zone. While alternative origins, such as diamond growth from mantle-derived fluids undergoing isotopic fractionation towards “crustal-like” values are possible (Palot et al., 2012, Cartigny et al., 2014), there is increasing evidence that already initial growth in ultra-deep diamonds occurred from fluids with crustal signatures. This evidence includes diamonds from Brazil (Walter et al., 2011, Palot et al., 2012, Burnham et al., 2015, 2016, Thomson et al., 2016a and b), West Africa (Palot et al., 2012, 2014), Australia (Tappert et al., 2009) and southern Africa (Deines et al., 1991, Tappert et al., 2005a and b, and Ickert et al., 2015; this study), which collectively indicate that fractionation has a minor effect on the fluid composition and that the isotopic signatures reflect original crustal sources. The clear inference is that crustal carbon and nitrogen are commonly subducted to deep asthenosphere and transition zone depths.

The formation of superdeep diamonds has been related to slab-derived carbonatitic melts reacting with peridotitic wall rock (Walter et al., 2008, Burnham et al., 2015, 2016, Thomson et al., 2016a and b). In this model, partial melting of former oceanic crust in the transition zone produces carbonatitic melts (the carbon filter model of Thomson et al., 2016a) and the subsequent interaction of these melts with ambient mantle is responsible for the formation of transition zone diamonds. Although such a model works well for ultra-deep diamonds from Juina, it is unlikely

311 for the Monastery and Jagersfontein diamonds based on trace elements (Moore et al., 1991,
312 Tappert et al., 1995b) and oxygen isotopic compositions (Ickert et al., 2015) of the majorite
313 inclusions. The $REE_N$ patterns of Monastery and Jagersfontein majoritic garnets (Fig. 9) overlap
314 closely with eclogitic garnets from lithospheric diamonds and xenoliths. A positive slope across
315 the $REE_N$ in Monastery and particularly pronounced, in Jagersfontein samples is not a feature of
316 Juina majorite inclusions, for which the Walter et al. (2008) model and subsequent variants are
317 valid. As a consequence, the $REE_N$ patterns of Monastery and Jagersfontein majorites cannot be
318 readily explained through reaction of a slab derived carbonatitic melt with peridotitic mantle. The
319 majoritic garnets here likely originate from broadly N-MORB-like precursors that have lost some
320 LREE and possibly experienced some HREE enrichment during partial melting in the garnet
321 stability field (Rapp and Watson, 1995; Rapp and Shimizu, 1998). The high $\delta^{18}O$ values of the
322 Jagersfontein majorite inclusions are also consistent with an eclogitic slab model and more
323 specifically with a hydrothermally weathered basaltic rock as a protolith (Ickert et al., 2015).
324 Hence, the preferred mechanism to form the Monastery and Jagersfontein super-deep diamonds is
325 by dissolution and re-precipitation, where subducted metastable graphite would be converted into
326 an oxidised or reduced species during fluid-aided dissolution, before being re-precipitated as
327 diamond (Ickert et al., 2015). This interpretation implies that, in this situation, carbon remains in
328 the subducting slab and is locally re-distributed to form sub-lithospheric diamonds beneath the
329 Kaapvaal Craton.

330 Taking into account the anomalous oxygen isotopic signatures of majorite garnets
331 reported from Juina (Burnham et al., 2015) and Jagersfontein (Ickert et al., 2015), we concur with
332 the numerous studies that document growth of ultra-deep diamonds from fluids derived from
333 mixtures of subducted organic matter and either surficial carbonate or mantle carbon. The $\delta^{13}C$
334 values of the Monastery and Jagersfontein ultra-deep diamonds are clearly more negative than

those from Juina and Kankan (Fig. 8) suggesting that their carbon source has a higher ratio of organic matter ($\delta^{13}C$ < -25‰) to either carbonate ($\delta^{13}C$ = 0‰) or mantle-derived carbon ($\delta^{13}C$ = -5‰). Using formation depth estimates constrained by garnet inclusion chemistry, there is also no apparent relationship between the depth of diamond formation and their isotopic composition, making the existence of a common, homogenous parent melt generating all ultra-deep diamonds during a single event for a given locality unlikely.

The positive $\delta^{15}N$ signatures of the southern African diamonds studied here are consistent with derivation from subducted nitrogen (Cartigny et al., 2014). The relatively low nitrogen content for the majority of the samples may reflect prior devolatilization of nitrogen during subduction (Busigny and Bebout, 2013) or perhaps nitrogen partitioning into a phase such as metal (Smith and Kopylova, 2014), which appears to play a role in the formation of some transition zone diamonds (Smith et al., 2016). Low N contents may also reflect a relatively nitrogen-poor protolith such as basaltic/gabbroic oceanic crust.

This study illustrates that both carbon and nitrogen are cycled from the surface deep into the asthenosphere and transition zone, underpinning other evidence for deep recycling of surficial volatile elements within the transition zone, documented in studies of diamonds from Brazil (Hutchison et al., 1999, Walter et al., 2011, Palot et al., 2012, Pearson et al., 2014 Burnham et al., 2015, Thomson et al., 2016), Guinea (Stachel et al., 2002, Palot et al., 2014), Jagersfontein (Tappert et al., 2005a, b, Ickert et al., 2015). The preponderance of recycled crustal materials in the transition zone may reflect a tendency of some subducted oceanic slabs to “pond” at this depth, depending on their thermal history (e.g., Ringwood, 1982; van der Hilst et al., 1997).

### 5.3 A diversity of diamond-forming fluids

Despite the fact that the ultra-deep Monastery and Jagersfontein diamonds point clearly to a subducted source for the carbon and nitrogen in their parental fluids, there is also evidence of variability among these fluids. Intra-diamond variability in $\delta^{13}$C-N-$\delta^{15}$N provides information about the nature of the diamond-forming fluids. In order to address this question we focus our attention on samples, which show smooth correlations of $\delta^{13}$C-N-$\delta^{15}$N and, based on CL-patterns, most likely represent coherent growth zones formed from single pulses of fluid. In contrast, the samples that exhibit complex growth layering in CL and have no apparent correlation of $\delta^{13}$C-N-$\delta^{15}$N will not be discussed in this section as they may result from a variety of processes (e.g. locally changing P-T-$fO_2$ or multiple episodes of growth from numerous fluid pulses).

The core-to-rim variations of the selected diamonds (see below) are best explained by equilibrium diamond growth from an evolving fluid, which underwent isotopic and elemental fractionation while diamond formed (Deines, 1980, Thomassot et al., 2007, Palot et al. 2014). The growth of diamond via either reduction of oxidized C-H-O-N fluid or oxidation of a reduced fluid phase leads to distinct systematic trends in C- and N-isotopic composition and N-abundance. The progress of isotopic fractionation is mainly a function of fluid speciation and temperature. Diamond is depleted in $^{13}$C by a few per mill compared to oxidised carbon at the temperatures of diamond formation ($CO_2$ and carbonate, Bottinga, 1969, Richet et al., 1977, Chacko et al., 1991, Polyakov and Kharlashina, 1995), leading to a core-to-rim increase in $^{13}$C as residual fluids progressively become relatively enriched in $^{13}$C. In contrast, diamond is enriched in $^{13}$C by a few per mill relative to reduced carbon species (carbide and $CH_4$, Richet, 1977, Satish-Kumar et al., 2011), leading to the opposite trend. Petts et al. (2015) suggested that the $CN^-$ molecule may be the best analogue for nitrogen speciation in diamond based on similar vibrational frequencies. At 1100°C, they estimated empirically that the nitrogen in diamond ($CN^-$

382 ) is depleted in $^{15}N$ by -3.6‰, -1.4‰ and -2.1‰ relative to $NH_4^+$, $NH_3$ and $N_2$, respectively,
383 leading to a core-to-rim increase in $^{15}N$.

384 Rayleigh fractionation best describes the co-variations between C-isotope composition
385 and other tracers such as N-isotope composition or [N] (Smart et al., 2011, Wiggers de Vries,
386 2013, Cartigny et al., 2014, Mikhail et al., 2014). The effects of this process on $\delta^{13}C$, $\delta^{15}N$ and
387 [N] can be described by the following equation (see Cartigny et al., 2014 and Petts et al., 2015 for
388 details)

389 $$(\delta^X) = (\delta^X)_0 + \Delta^X_{\text{diam-fluid}} \times \ln f_X$$

390 where $f_X$ is the remaining fraction of carbon/nitrogen in the diamond forming medium (in
391 the scenario where diamond crystallizes from a fluid entirely made up of carbon species $f_C$ =
392 fraction of fluid consumed), $\delta^X_0$ is the initial carbon/nitrogen isotopic composition of the fluid,
393 and $\Delta^X$ is the fractionation factor of carbon/nitrogen between diamond and the fluid growth
394 medium.

395 The carbon isotopic composition of the fluid is related to N-abundance (i.e. N/C) by the
396 following equation:

397 $$\ln(N/C) = \ln(N/C)_0 + \left[\frac{\left(\delta^{13}C - \delta^{13}C_0\right)}{K_C \times \Delta C}\right] \times \left(\frac{K_N}{K_C} - 1\right)$$

398 where $(N/C)_0$ is the initial nitrogen abundance in the fluid. $K_N$ is a measure of the
399 compatibility of nitrogen during diamond growth (with $K_N < 1$ for incompatible and $K_N > 1$ for
400 compatible behaviour). $K_C$ is the partition coefficient for carbon (in the case of diamond growth
401 Kc = 1). $\delta^{13}C_0$ is the initial carbon isotopic composition of the fluid.

402 Modelled geochemical parameters ($\delta^{13}C_0$, $\delta^{15}N_0$, $N/C_0$, $K_N$ and $\Delta C$) have been
403 determined to fit the variations in $\delta^{13}C$-$\delta^{15}N$-[N] (Figs. 4-7). Comparison of the estimated

404 magnitude of isotopic fractionation of carbon and nitrogen with theoretical calculations,
405 experimental data and observation in natural diamonds therefore help us to constrain the nature of
406 the diamond-forming fluids.
407
408 **5.3.1 Diamond growth from an oxidised carbon phase**
409 Diamonds Mon B9-07, JF09, JF44 and JF50 exhibit progressive $^{13}C$ enrichment from core
410 to rim (Figs. 4, 5 and 7). Modelling of the $\delta^{13}C$-$\delta^{15}N$-[N] co-variations in these diamonds yields
411 negative fractionation factors for $\Delta C_{diamond\text{-}fluid}$ = -2.8 to -1.0‰ (i.e. diamond is $^{13}C$ depleted
412 relative to fluid; Table 4). We illustrate in Fig. 10 the $\Delta C$ of these studied diamonds together with
413 the theoretical/expected values for diamond in equilibrium with both oxidised and reduced
414 carbon species (Bottinga, 1969, Richet et al., 1977, Chacko et al., 1991, Polyakov and
415 Kharlashina, 1995). The temperatures of isotopic equilibrium have been estimated using the
416 pressure estimates of majorite formation/equilibration extrapolated to a typical mantle geotherm
417 (Katsura et al., 2010; Table 1). The exact magnitude of such fractionation factors may be
418 inaccurate if these diamonds formed in a "young", non-thermally equilibrated subducted slab that
419 foundered in the transition zone. In this case the fractionation factors would move towards more
420 negative values for oxidised carbon species and more positive values for reduced carbon forms.
421 Although it is not possible to constrain the exact nature of the diamond-forming fluid
422 (pure end-member vs multi-component fluid) from the current data, it is clear that at least some
423 diamonds from Monastery and Jagersfontein formed from oxidised fluids. The formation of ultra-
424 deep diamonds from oxidised source fluids has been suggested based on the observation of
425 carbonate inclusions within ultra-deep diamonds from Brazil (Wirth et al., 2009, Bulanova et al.,
426 2010) and Kankan (Brenker et al., 2005), and the growing geochemical and experimental

evidence for the percolation of carbonatitic melts in the deep mantle (Walter et al., 2008, Burnham et al., 2015, 2016, Thomson et al. 2016a and b).

Modelling the behaviour of nitrogen for these diamonds during their formation yields $K_N$ = 6.0-10.0, with strong partitioning of nitrogen into diamond for all samples (Table 4). The magnitude of $K_N$ appears to be independent of pressure and likely relates to fluid compositions. An exclusively compatible behaviour of nitrogen ($K_N$ = 4-16) was also observed for ultra-deep diamonds from Kankan, which formed from both oxidised and reduced fluids (Palot et al., 2014).

### 5.3.2 Diamond growth from reduced carbon species

Diamonds Mon A4-03 and JF58 exhibit progressive $^{13}C$ depletion from core to rim (Fig. 6), leading to positive fractionation factors $\Delta C_{diamond\text{-}fluid}$ = +1.2 and +1.5‰ (i.e. diamond is $^{13}C$ enriched compared to fluid; Table 4, Fig. 10). Such values are consistent with equilibrium between diamond and reduced carbon species (Richet, 1977, Satish-Kumar et al., 2011). Again we cannot resolve whether the fluid is a pure end-member or a mix between several reduced carbon fluid species (e.g., $C_2H_6$ & $CH_4$).

Methane and diamond are predicted to be the dominant carbon species in the deep asthenosphere (Frost and McCammon, 2008). The observation of micro-inclusions of $CH_4$ in Marange diamonds demonstrates that $CH_4$-rich fluids exist even at lithospheric depths (Smit et al., 2016). The discovery of carbide and native iron as inclusions in ultra-deep diamonds (Kaminsky and Wirth, 2011, Kaminsky, 2012; Smith et al., 2016), including those from Jagersfontein (Mikhail et al., 2014), document reducing conditions in parts of the deep mantle – from the deep asthenosphere to the uppermost lower mantle. Models predict metal saturation at 250-300 km depth in the mantle, where carbon forms carbide in metal (e.g. Frost and McCammon, 2008). The formation of diamond from carbon-iron melt may thus not be restricted

to the lower mantle (Kaminsky and Wirth, 2011) but may also occur (locally?) within the asthenosphere/transition zone, as documented by metal-dominated mineral assemblages in large ultra-deep diamonds (Smith et al., 2016). Owing to the scarcity of these assemblages in natural samples, we can, however, not exclude that they may reflect extremely localised environments.

The estimated nitrogen partition coefficient between these 2 samples and their parental C-H-O-N fluids is restricted to $K_N$ = 0.3-0.7. This contrasts with estimates of other diamonds supposedly in equilibrium with $CH_4$ fluid ($K_N$ = 2 and 8 in Thomassot et al., 2007 and Palot et al., 2013 respectively).

Ultra-deep diamonds from Jagersfontein and Monastery add to the evidence provided by ultra-deep diamonds from Juina and Kankan in showing that diamonds within the deep asthenosphere and transition zone can form from both oxidised and reduced fluids, suggesting that diamond could be one of the dominant carbon species in this part of the Earth.

### 5.3.3 Diamond-forming fluids involving reduced nitrogen species

Diamond Mon B9-07, which formed from oxidised fluids, also shows core-to-rim $^{15}N$ enrichment (Fig. 4). Modelling of the $\delta^{15}N$-[N] variations of this diamond yields nitrogen fractionation factor $\Delta N_{diamond\text{-}fluid}$ of -3.0‰ (Table 4, Fig. 11). Such a preferential incorporation of $^{15}N$ in diamond over the diamond-forming fluid (i.e. negative $\Delta N_{diamond\text{-}fluid}$) has been previously observed in lithospheric diamonds from Jericho (Petts et al., 2015) and ultra-deep diamonds from Kankan (Palot et al., 2014). The isotopic equilibrium between $CN^-$ (as an analogue for nitrogen in diamond – see discussion in Petts et al., 2015) and reduced nitrogen species ($N_2$, $NH_3$ and $NH_4^+$) has been used here in order make a self-consistent comparison.

At $T_{inclusion}$ of 1550°C (majorite-derived barometry projected onto the mantle adiabat), the empirical $\Delta N_{diamond\text{-}fluid}$ of -3.0‰ is in closer agreement to the theoretical fractionation factor of $CN^- - NH_4^+$ ($\Delta_{CN\text{-}NH4}$ = -2.5‰, Petts et al., 2015) than with the theoretical fractionation factor for $CN^- - N_2$ ($\Delta_{CN\text{-}N2}$ = -1.4‰, Petts et al., 2015). If our samples formed within a colder environment than convecting mantle such as a subducting slab, the Mon B9-07 point would be shifted toward the $CN^- - NH_4^+$ curve. The magnitude of $\Delta_{Mon\ B9\text{-}07\text{-}fluid}$ is close to estimates for diamonds from Jericho (Petts et al., 2015), where the source of nitrogen has been proposed to be $NH_4^+$ molecules. However, due to the relative large uncertainty in estimating the nitrogen fractionation factor here (which is not quantifiable at the present time), we cannot exclude the possibility that both diamond forming-fluids contain significant amounts of $NH_3$ (see discussion in Petts et al., 2015).

Thermodynamic calculations (Mikhail and Sverjensky, 2014) predict nitrogen predominantly in the form of $N_2$ in fluids existing under oxidized conditions (e.g., mantle wedges at convergent plate margins, or in the carbonate melts emanating from deeply subducted slabs, e.g., Thomson et al., 2016a), or as $NH_4^+$ in aqueous fluids in equilibrium with more reducing conditions (e.g. Mikhail and Howell, 2016). In a recent study, Mikhail et al., (2017) have shown the relationship between pH (in addition to temperature, pressure, oxygen fugacity and chemical activity) and nitrogen speciation in the mantle, illustrating the complexity of parameters that control speciation. Such calculations may not be applicable to our ultra-deep samples as temperatures for the Mikhail et al., (2017) calculations did not exceed 1000°C but further investigation with extended temperatures and pressure would help to resolve this issue. $NH_4^+$ is also a dominant nitrogen species in the crust because of its common substitution for $K^+$ in clays, micas, feldspars, clinopyroxenes and amphiboles (e.g. Watenphul et al., 2010, Busigny and Bebout, 2013). This substitution of nitrogen into minerals with a large stability range establishes

497 a mechanism for transporting nitrogen into the deep mantle during subduction and strengthens
498 our interpretation of a subduction origin of the studied sample suite.

499 Estimates of $K_N$ ranging from 6.5 to 6 for JF50 and Mon B9-07, respectively, indicate that
500 nitrogen is strongly concentrated in diamond, making it an important carrier for nitrogen in the
501 asthenosphere/transition zone.

502

503 **5.2 Implication for the deep carbon and nitrogen cycle**

504 The carbon and nitrogen isotopic signatures of the Monastery and Jagersfontein super-
505 deep diamonds indicate the recycling of these elements in the asthenosphere/transition zone.
506 Systematic higher temperatures of ultra-deep diamond formation ($T_{inclusion}$) compared to time
507 averaged mantle residence temperatures ($T_{N\text{-}aggregation}$) (Table 1), suggest that the studied
508 diamonds have experienced short residence in the "hot" asthenosphere/transition zone. Such a
509 short mantle residence time is fully consistent with the fact that most of these diamonds are not
510 100% aggregated. Using the N systematics (35%B and 20 at.ppm N) of the least aggregated
511 diamond (Mon B9-07) and assuming a residence temperature of 1480°C (for the appropriate
512 depth in the convective mantle transition zone) this sample resided for <1Ma before exhumation
513 either to Earth's surface or to intermediate storage in a relatively "cool" lithospheric
514 environment. If these diamonds formed in a cooler slab environment, this would be a minimum
515 estimate. However, it would still require that the diamonds were picked up from the slab and
516 transported upwards fairly rapidly, before the subducted slab could thermally equilibrate with the
517 surrounding mantle. These estimates contrast with the Proterozoic Re-Os sulphide ages for
518 lithospheric eclogitic diamonds from the Jagersfontein mine (Aulbach et al., 2009), suggesting
519 that ultra-deep diamonds form in a different way than lithospheric diamonds.

Rapid vertical movement to shallower mantle conditions is consistent with the observation of i) un-retrogressed hydrous ringwoodite in a Juina diamond (Pearson et al., 2014; ii) only partially unmixed inclusions in diamonds coming from the transition zone in Kankan and Juina (e.g. Harte and Cayzer, 2007) and iii) modeling of the diffusive relaxation of carbon isotope heterogeneity in ultra-deep diamonds from Kankan (Palot et al., 2014). The unexsolved nature of the majorite inclusions in our sample suite is consistent with these observations. Combined, these observations lend strong support to the notion that some component of the transporting kimberlitic magmas originates in, or below, the transition zone. It can, however, not be ruled out that ultra-deep diamonds may also be transported by exceptionally vigorous convective mantle flow (Palot et al., 2012, Tappe et al., 2013). The observation of ubiquitous crustal signatures in the mantle transition zone raises the question of the importance of this region in terms of the global carbon budget. Kelemen and Manning (2015) emphasise the efficiency of the subduction zone "filter" in preventing carbon to go into the deeper convecting mantle. The ultra-deep diamonds studied here and from other localities clearly indicate a provenance from crustal protolith-derived fluids within the deep upper mantle and transition zone, but it is likely that this inventory of crustal carbon is relatively small. Kelemen and Manning (2015) estimate the total amount of carbon in the mantle sampled by all kimberlites as ~3 x $10^5$ Mt and make the broad assumption that this inventory reflects only recycled carbon. Nonetheless, this provides a first order estimate and translates to a mass fraction of ~ 3.3 x $10^{-6}$ of the subducted crustal carbon reservoir. Even this may be an over-estimate for the carbon in the transition zone, but it is difficult to improve on the estimate without some additional gross assumptions. If we assume either that only 2% of kimberlites sample super-deep diamonds, or, that all Type II diamonds, that represent ~2% of all diamonds, are of super-deep origin (Smith et al., 2016) then only ~ 6 x $10^3$ Mt of carbon (0.66 billionth of the crustal reservoir mass) might exist within transition zone-

hosted diamonds. This estimate is highly uncertain but places a lower bound on the flux of recycled carbon into the deep mantle. A further complicating issue is the fact that metallic Fe in the transition zone appears to form C alloys such as cohenite (Smith et al., 2016) and some of the diamonds analysed here may have equilibrated with such alloys. In a highly reduced and moderately hydrous environment, carbon would preferentially partition into silicate melt relative to metal alloy (Li et al., 2015). Despite these complications, it seems likely that the transition zone is a carbon and nitrogen reservoir dominated by recycled crustal components.

## 6. Conclusions

The systematically $^{13}C$ depleted and $^{15}N$ enriched signatures in ultra-deep Monastery and Jagersfontein diamonds indicate that they crystallised from fluids derived from subducted material. These findings illustrate deep cycling of surficial carbon and nitrogen into the asthenosphere and transition zone. Combined C- and N- isotopic data across growth sections of the diamonds support repeated diamond growth via metasomatic processes. Modelling of the internal co-variations in $\delta^{13}C$-$\delta^{15}N$-N reveals that the diamonds grew from a variety of C-H-O-N fluids, involving both oxidised and reduced species. Our data support the idea that subducted oceanic slabs tend to pond at transition zones depths, where carbon mobilized both as oxidised and reduced species is re-precipitated locally as diamond. Recycled volatiles may dominate the Earth's transition zone.

## Acknowledgements

R.O Moore is thanked for generously providing part of the studied samples. This study was co-funded by the Canada Excellence Research Chair Program. The Canadian Center for Isotopic

Microanalysis (CCIM) was created through CFI and ASRIP grants to T.S. This is CCIM contribution XXX.

## References


1. Aulbach S., Shirey S.B., Stachel T., Creighton S., Muehlenbachs K., Harris J.W., 2009. Diamond formation episodes at the southern margin of the Kaapvaal Craton; Re-Os systematics of sulfide inclusions from the Jagersfontein Mine. *Contrib Mineral Petrol* **157**, 525-540, doi: 10.1007/s00410-008-0350-9.
2. Barry, P. and Hilton, D.R., 2016. Release of subducted sedimentary nitrogen throughout Earth's mantle. *Geochemical Perspectives Letters* **2**, 148-159 doi: 10.7185/148 geochemlet.1615.
3. Bulanova, G.P., Pearson, D.G., Hauri, E.H., Griffin, B.J., 2010. Carbon and nitrogen isotope systematics within a sector-growth diamond from the Mir kimberlite, Yakutia. *Chem. Geol* **188**, 105-123.
4. Bulanova, G.P., Walter, M.J., Smith, C.B., Kohn, S.C., Armstrong, L.S., Blundy, J., Gobbo, L., 2010. Mineral inclusions in sublithospheric diamonds from Collier 4 kimberlite pipe, Juina, Brazil: subducted protoliths, carbonated melts and primary kimberlite magmatism. *Contrib. Mineral. Petrol.* **160**, 489–510.
5. Burhnam, A.D., Thomson, A.R., Bulanova, G.P., Kohn, S.C., Smith, C.B., Walter, M.J., 2015. Stable isotope evidence for crustal recycling as recorded by superdeep diamonds. *Earth Planet. Sc. Lett.* **432**, 374-380.
6. Burnham, A.D., Bulanova, G.P., Smith, C.B., Whitehead, S.C., Kohn, S.C., Gobbo, L., Walter, M.J., 2016. Diamonds from the Machado River alluvial deposit, Rondônia, Brazil, derived from both lithospheric and sublithospheric mantle. *Lithos* **265**, 199-213.
7. Busigny, V., Bebout, G.E., 2013. Nitrogen in the silicate Earth: Speciation and isotopic behavior during mineral–fluid interactions. *Elements* **9**, 353-358.
8. Bottinga, Y., 1969. Carbon isotope fractionation between graphite, diamond and carbon dioxide. *Earth Planet. Sc. Lett.* **5**, 301-307.
9. Boyd, S. R., Kiflawi, I., and Woods, G.S., 1994b. The relationship between infrared absorption and the A defect concentration in diamond. Philos. Mag. 69, 1149-1153.
10. Boyd, S. R., Kiflawi, I., and Woods, G.S., 1995. Infrared absorption by the B nitrogen aggregate in diamond. Philos. Mag. 72, 351-361.
11. Brenker, F. E., Vincze, L., Vekemans, B., Nasdala, L., Stachel, T., Vollmer, C., Kersten, M., Somogyi, A., Adams, F., Joswig, W., and Harris, J. W., 2005. Detection of a Ca-rich lithology in the Earth's deep (>300 km) convecting mantle. *Earth Planet. Sc. Lett.* **236**, 579-587.
12. Cartigny, P., Marty, B., 2013. Nitrogen isotopes and mantle geodynamics: The emergence of life and the atmosphere– crust–mantle connection. *Elements* **9**, 359-366

13. Cartigny, P., Palot, M., Thomassot, E., Harris, J.W., 2014. A stable isotope perspective on the formation of diamonds and its link to mantle chemical geodynamics and oxidation states. *Ann. Rev. Earth Planet. Sci. Lett.* **42**, 699-732.

14. Chacko, T., Mayeda, T. K., Clayton, R. N., and Goldsmith, J. R., 1991. Oxygen and carbon isotope fractionations between $CO_2$ and calcite. *Geochim. Cosmochim. Acta.* **55**, 2867-2882.

15. Dasgupta, R. and Hirschmann, M. M., 2010. The deep carbon cycle and melting in Earth's interior. *Earth Planet. Sci. Lett.* **298**, 1-13.

16. Dasgupta, R., Hirschmann, M.M., and Withers, A., 2004. Deep global cycling of carbon constrained by the solidus of anhydrous, carbonated eclogite under upper mantle conditions. *Earth Planet. Sci. Lett.* **227**, 73-85.

17. Deines, P., Harris, J.W., Gurney, J.J., 1991. The carbon isotopic composition and nitrogen content of lithospheric and asthenospheric diamonds from the Jagersfontein and Koffiefontein kimberlite, South Africa. *Geochim. Cosmochim. Ac.* **55**, 2615-2625.

18. Duit, W., Jansen, J.B.H., Van Breemen, A., Bos, A., 1986. Ammonium micas in metamorphic rocks as exemplified by Dome de l'Agout (France). *American Journal of Science* **286**, 702-732.

19. Dziewonski A.M. and Anderson D.L. 1981. Preliminary reference Earth model. *Phys Earth Planet Int* **25**, 297–356.

20. Frost, D. J. and McCammon, C. A., 2008. The redox state of Earth's mantle. *Ann. Rev. Earth Planet. Sci. Lett.* **36**, 389-420.

21. Gurney, J.J., Harris, J.W., Rickard, R.S., 1984. Silicate and oxide inclusions in diamonds from the Orapa mine, Botswana. In: Kornprobst, J. (Ed.), Kimberlites II: The Mantle and Crust-Mantle Relationships. Elsevier, Amsterdam, pp. 3–9.

22. Haggerty, S.E., 1986. Diamond Genesis in a Multiply-Constrained Model. *Nature* **320** (6057), 34-37.

23. Halama R, Bebout GE, John T, Schenk V., 2010. Nitrogen recycling in subducted oceanic lithosphere: the record in high and ultrahigh-pressure metabasaltic rocks. *Geochim. Cosmochim. Acta*. **74**, 1636-1652.

24. Harte, B., Cayzer, N., 2007. Decompression and unmixing of crystals included in diamonds from the mantle transition zone. *Physics and Chemistry of Minerals* **34**, 647–656.

25. Harte, B., Hudson, N.F.C., 2013. Mineral associations in diamonds from the lowermost upper mantle and uppermost lower mantle. *Proceedings of 10th International Kimberlite Conference*. Springer India, New Delhi, pp. 235–253. http://dx.doi.org/10.1007/978-81-322-1170-9_15.

26. Hutchison, M.T., Cartigny, P., and Harris, J.W., 1999. Carbon and Nitrogen Compositions and Physical Characteristics of Tranzition Zone and Lower Mantle Diamonds from São Luiz, Brazil Proceeding of the 7th International Kimberlite Conference. Red Rood Design, Cape Town.

27. Ickert, R.B., Stachel, T., Stern, R.A., Harris, J.W., 2015. Extreme $^{18}$O-enrichment in majorite constrains a crustal origin of transition zone diamonds. *Geochem. Persp. Let.* **1**, 65-74 doi: 10.7185/geochemlet.1507.

28. Irifune, T., 1987. An experimental investigation of the pyroxene-garnet transformation in a pyrolite composition and its bearing on the constitution of the mantle. *Phys. Earth Planet. Int.* **45**, 324-336.

643 29. Javoy, M., Pineau, F., Delorme, H., 1986. Carbon and nitrogen isotopes in the mantle. *Chem. Geol.*
644 **57**, 41–62.

645 30. Kaminsky, F. V., 2012. Mineralogy of the lower mantle: A review of "super deep" mineral
646 inclusions in diamond. *Earth-Science Reviews* **110**, 127-147.

647 31. Kaminsky, F. W. and Wirth, R., 2011. Iron carbide inclusions in lower mantle diamond from Juina,
648 Brazil. *The Canadian Mineralogist* **49**, 555-572.

649 32. Katsura, T., Yoneda, A., Yamazaki, D., Yoshino, T., Ito, E., 2010. Adiabatic temperature profile in
650 the mantle. *Physics of the Earth and Planetary Interiors* **18**, 212-218.

651 33. Kelemen P.B. and Manning, C.E., 2015. Reevaluating carbon fluxes in subduction zones, what
652 goes down, mostly comes up. *PNAS* **112 no. 30** doi: 10.1073/pnas.1507889112.

653 34. Klein-BenDavid, O., Pearson, D.G., Nowell, G., M., Ottley, C., McNeill, J.C.R., Logvinova, A.,
654 Sobolev, N.V., 2014. The sources and time-integrated evolution of diamond-forming fluids – Trace
655 elements and isotopic evidence. *Geochim. Cosmochim. Ac.* **125**, 146-169.

656 Li, Y., Dasgupta, R. and Tsuno, K., 2015. The effects of sulfur, silicon, water, and oxygen fugacity
657 on carbon solubility and partitioning in Fe-rich alloy and silicate melt systems at 3 GPa and
658 1600°C: Implications for core-mantle differentiation and degassing of magma oceans and reduced
659 planetary mantles. *Earth and Planetary Science Letters* **415**, 54-66.

660 35. McDonough, W.F. and Sun, S.-S., 1995. Composition of the Earth. *Chemical Geology* **120**: 223-
661 253.

662 36. Mikhail, S., Barry, P.H., Sverjensky, D.A.The relationship between mantle pH and the deep
663 nitrogen cycle. *GCA* **209**, 149-160.

664 37. Mikhail, S., Dobosi, G., Verchovsky, A.B., Kurat, G., Jones, A.P., 2013. Peridotitic and websteritic
665 diamondites provide new information regarding mantle melting and metasomatism induced
666 through the subduction of crustal volatiles. *Geochim. Cosmochim. Acta* **107**, 1–11.

667 38. Mikhail, S., Guillermier, C., Franchi, I., Beard, A., Krispin, C., Verchovsky, A., Jones, A. and
668 Milledge, H. J., 2014. Empirical evidence for the fractionation of carbon isotopes between
669 diamond and iron carbide from the Earth's mantle. *Geochem. Geophy. Geosys.* **15**, 855-866.

670 39. Mikhail, S. and Sverjensky, D.A., 2014. Nitrogen speciation in upper mantle fluids and the origin
671 of Earth's nitrogen-rich atmosphere. *Nat. Geo.* **7**, 816-819.

672 40. Mikhail, S. and Howell, D., 2016. A Petrological assessment of diamond as a recorder of the
673 mantle nitrogen cycle. *Am. Mineral.* **101**, 780-787.

674 41. Moore, R.O., Gurney, J.J., 1985. Pyroxene solid solution in garnets included in diamond. *Nature*
675 **318**, 553-555.

676 42. Moore, R.O., Gurney, J.J., Griffin, W.L., Shimizu, N., 1991. Ultra-high pressure garnet inclusions
677 in monastery diamonds: trace element abundance patterns and conditions of origin. *Eur. J.*
678 *Mineral.* **3**, 213-230.

679 43. Palot, M., Cartigny, P., Harris, J. W., Kaminsky, F. V., and Stachel, T., 2012. Evidence for deep
680 mantle convection and primordial heterogeneity from nitrogen and carbon stable isotopes in
681 diamond. *Earth Planet. Sci. Lett.* **357-358**, 179-193.

682 44. Palot, M., Cartigny, P., and Viljoen, K. S., 2009. Diamond origin and genesis: A C and N stable

isotope study on diamonds from a single eclogitic xenolith (Kaalvallei, South Africa). *Lithos* **112S**, 758-766.

45. Palot, M., Pearson, D. G., Stern, R. A., Stachel, T., and Harris, J. W., 2013. Multiple growth events, processes and fluid sources involved in diamond genesis: a micro-analytical study of sulphide-bearing diamonds from Finsch mine, RSA. *Geochim. Cosmochim. Acta* **106**, 51-70.

46. Palot, M., Pearson, D.G., Stern, R.A., Stachel, T., Harris, J.W., 2014. Isotopic constraints on the nature and circulation of deep mantle C-H-O-N fluids: carbon and nitrogen systematics within super deep diamonds from Kankan (Guinea). *Geochim. Cosmochim. Acta* **139**, 26-46.

47. Palot, M., Jacobsen, S.D., Townsend, J.P., Nestola, F., Marquardt, K., Harris, J.W., Stachel, T., McCammon, C.A., Pearson, D.G. 2016. Evidence for $H_2O$-bearing fluids in the lower mantle from diamond inclusion. *Lithos* **265**, 237-243.

48. Pearson, D.G., Brenker, F.E., Nestola, F., McNeill, J., Nasdala, L., Hutchison, M., Matveev, S., Mather, K., Silversmit, G., Schmitz, S., Vekemans, B., Vincze, L., 2014. Hydrous mantle transition zone indicated by ringwoodite included within diamond. *Nature* **507**, 221-224.

49. Petts, D.C., Chacko, T., Stachel, T., Stern, R.A., Heaman, L.M., 2015. A nitrogen isotope fractionation factor between diamond and its parental fluid derived from detailed SIMS analysis of a gem diamond and theoretical calculations. *Chem. Geol.* **410**, 188-200.

50. Petts, D.C., Stachel, T., Stern, R.A., Hunt, L., Foradas, G., 2016. Multiple carbon and nitrogen sources associated with the parental mantle fluids of fibrous diamonds from Diavik, Canada, revealed by SIMS microanalysis. *Contrib. Mineral. Petrol.* **171:17** DOI 10.1007/s00410-016-1231-2.

51. Polyakov, V. B. and Kharlashina, N. N., 1995. The use of heat capacity data to calculate carbon isotope fractionation between graphite, diamond, and carbon dioxide : A new approach. *Geochim. Cosmochim. Acta.* **59**, 2561-2572.

52. Rapp, R.P., Shimizu, N., 1998. Subduction and slab melting in the Archean: experimental constraints and implications for the development of cratonic lithosphere., Seventh International Kimberlite Conference, Cape Town, pp. 720-722.

53. Rapp, R.P., Watson, E.B., 1995. Dehydration melting of metabasalt at 8-32-kbar - Implications for continental growth and crust-mantle recycling. *J. Petrol.* **36**, 891-931.

54. Richet, P., Bottinga, Y., and Javoy, M., 1977. A review of hydrogen, carbon, nitrogen, oxygen, sulphur and chlorine stable isotope fractionation among gaseous molecules. *Ann. Rev. Earth Planet. Sci. Lett.* **82**, 269-279.

55. Ringwood, A.E., 1982 Phase transformations and differentiation in subducted lithosphere: implications for mantle dynamics, basalt petrogenesis, and crustal evolution. *The journal of Geology* **90, No. 6**, 611-643.

56. Satish-Kumar, M., So, H., Yoshino, T., Kato, M., Hiroi, Y., 2011. Experimental determination of carbon isotope fractionation between iron carbide melt and carbon: $^{12}$C-enriched carbon in the Earth's core? *Earth Planet. Sc. Lett.* **310**, 340-348.

57. Schrauder M, Navon O., 1993. Solid carbon dioxide in a natural diamond. *Nature* **365**:42–44.

58. Schulze, D.J., Wiese, D., Steude, J., 1996. Abundance and distribution of diamonds in eclogite revealed by volume visualization of CT X-ray scans. *J. Geol.* **104**:109–13.

59. Schulze, D.J., 2003. A classification scheme for mantle-derived garnets in kimberlite: a tool for investigating the mantle and exploring for diamonds. *Lithos* **71**, 195-213.

60. Shirey, S.B., Cartigny, P., Frost, D.J., Keshav, S., Nestola, F., Nimis, P., Pearson, D.G., Sobolev, N., Walter, M.J., 2013. Diamonds and the geology of mantle carbon. *Rev. Mineral. Geochem.* **75**, 355-421.

61. Smart, K.A., Chacko, T., Stachel, T., Muehlenbachs, K., Stern, R.A., Heaman, L.M., 2011. Diamond growth from oxidized carbon sources beneath the Northern Slave Craton, Canada A $\delta^{13}$C-N study of eclogite-hosted diamonds from the Jericho kimberlite. *Geochim. Cosmochim. Acta*. **75**, 6027-6047.

62. Smart, K.A., Tappe, S., Stern, R.A., Webb, S.J., Ashwal, L.D., 2016. Early Archean tectonics and mantle redox recorded in Witwatersrand diamonds. *Nat. Geo*. **9**, 255-259.

63. Smit, K.V., Shirey, S.B., Stern, R.A., Steele, A., Wang, W., 2016. Diamond growth from C-H-N-O fluids in the lithosphere: evidence from $CH_4$ micro-inclusions and $\delta^{13}$C- $\delta^{15}$N-N content in Zimbabwe mixed-habit diamonds. *Lithos* **265**, 68-81.

64. Smith, E.M., Shirey, S.B., Nestola, F., Bullock, E.S., Wang, J., Richardson, S.H., Wang., W., 2016. Origin of big gem diamonds from metallic liquid in deep Earth mantle. *Science* **354**, 1403-1405.

65. Smith, E. M. and Kopylova, M. G., 2014 Implications of metallic iron for diamonds and nitrogen in the sublithospheric mantle. *Canadian Journal of Earth Sciences* **51**, 510-516.

66. Sobolev, N.V., Snyder, G.A., Taylor, L.A., Keller, R.A., Yefimova, E.S., et al. 1998. Extreme chemical diversity in the mantle during eclogitic diamond formation: evidence from 35 garnet and 5 pyroxene inclusions in a single diamond. *Int. Geol. Rev.* **40**, 567–78.

67. Stachel, T., Aulbach, S., Brey, G.P., Harris, J.W., Leost, I., Tappert, R., Viljoen, K.S., 2004. The trace element composition of silicate inclusions in diamonds: a review. *Lithos* **77**, 1–19.

68. Stachel, T., Brey, G. P., and Harris, J. W., 2005. Inclusions in Sublithospheric Diamonds : Glimpses of Deep Earth. *Elements* **1**, 73-78.

69. Stachel, T. and Harris, J. W., 2008. The origin of cratonic diamonds - Constraints from mineral inclusions. *Ore Geology Reviews* **34**, 5-32.

70. Stachel, T., Harris, J. W., Aulbach, S., and Deines, P., 2002. Kankan diamonds (Guinea) III : $\delta^{13}$C and nitrogen characteristics of deep diamonds. *Contrib. Mineral. Petrol.* **142**, 465-475.

71. Stachel, T., Harris, J.W., Muehlenbachs, K., 2009. Sources of carbon in inclusion bearing diamonds. *Lithos* **112S**, 625-637.

72. Stern, R.A., Palot, M., Howell, D., Stachel, T., Pearson, D.G., Cartigny, C., Oh, A., 2014. Methods and reference materials for SIMS diamond C- and N-isotope analysis. *era.library.ualberta.ca. URL*. http://hdl.handle.net/10402/era.38738.

73. Taylor, W.R., Jaques, A.L., Ridd, M., 1990. Nitrogen-defect aggregation characteristics of some Australian diamonds: time–temperature constraints on the source regions of pipe and alluvial diamonds. *American Mineralogist* **75**, 1290–1310.

1. Taylor, L.A., Snyder, G.A., Crozaz, G., Sobolev, V.N., Yefimova, E.S., Sobolev, N.V., 1996. Eclogitic inclusions in diamonds: evidence of complex mantle processes over time. *Earth Planet. Sci. Lett.* **142**, 535–551.

2. Tappe, S., Pearson, D. G., Kjarsgaard, B. A., Nowell, G., Dowall, D., 2013. Mantle transition zone input to kimberlite magmatism near a subduction zone: Origin of anomalous Nd–Hf isotope systematics at Lac de Gras, Canada. *Earth Planet. Sci. Lett.* **371-372**, 235–251.

3. Tappert, R., Stachel, T., Harris, J.W., Muehlenbachs, K., Ludwig, T., Brey, G.P., 2005a. Subducting oceanic crust: The source of deep diamonds. *Geology* **33**, 565-568.

4. Tappert, R., Stachel, T., Harris, J.W., Muehlenbachs, K., Ludwig, T., Brey, G.P., 2005b. Diamonds from Jagersfontein (South Africa): messengers from the sublithospheric mantle. *Contrib. Mineral. Petrol.* **150**, 505-522.

5. Thomassot, E., Cartigny, P., Harris, J.W., Vijoen, K.S., 2007. Methane-related diamond crystallization in the Earth's mantle: Stable isotope evidences from a single diamond-bearing xenolith. *Earth Planet. Sci. Lett.* **257**, 362-371.

6. Thomson, A.R., Walter, M.J., Kohn, S.C., Brooker, R.A., 2016a. Slab melting as a barrier to deep carbon subduction. *Nature* **529**, 76–79.

7. Thomson, A.R., Kohn, S.C., Bulanova, G. P., Smith, C.B., Araujo, D., Walter, M.J., 2016b. Trace element composition of silicate inclusions in sub-lithospheric diamonds from the Juina-5 kimberlite: Evidence for diamond growth from slab melts. *Lithos* **265**, 108-124.

8. Van der Hilst, R. D., Widiyantoro, S., Engdahl, E. R. Evidence for deep mantle circulation from global tomography. *Nature* **386**, 578-584.

9. Wagner, P.A. 1914. The diamond fields of southern Africa, *in: Transvaal Leader, xxv, Johannesburg*, pp. 347.

10. Walter, M. J., Bulanova, G. P., Armstrong, L. S., Keshav, S., Blundy, J. D., Gudfinnsson, G., Lord, O. T., Lennie, A. R., Clark, S. M., Smith, C. B., and Gobbo, L., 2008. Primary carbonatite melt from deeply subducted oceanic crust. *Nature* **454**, 622-626.

11. Walter, M. J., Kohn, S. C., Araujo, D. Bulanov, G.P., Smith, C.B., Gaillou, E., Wang, J., Steele, A., Shirey, S.B., 2011. Deep Mantle Cycling of Oceanic Crust: Evidence from Diamonds and Their Mineral Inclusions. *Science* **334**, 54-57.

12. Watenphul, A., Wunder, B., Wirth, R., Heinrich, W., 2010. Ammonium-bearing clinopyroxene: A potential nitrogen reservoir in the Earth's mantle. *Chemical Geology* **270**, 240-248.

13. Weiss, Y., McNeill, J., Pearson, D.G., Nowell, G.M., Ottley, C.J., 2015. Highly saline fluids from a subducting slab as the source for fluid-rich diamonds. *Nature* **524**, 339-342.

14. Wijbrans, C.H., Rohrbach, A., Klemme, S., 2016. An experimental investigation of the stability of majoritic garnet in the Earth's mantle and an improved majorite geobarometer. *Contrib. Mineral. Petro.* **171:50**, DOI 10.1007/s00410-016-1255-7.

15. Wiggers de Vries, D.F., Pearson, D.G., Bulanova, G.P., Smelov, A.P., Pavlushin, A.D., Davies, G.R., 2013. Re-Os dating of sulphide inclusions zonally distributed in single Yakutian diamonds: Evidence for multiple episodes of Proterozoic formation and protracted timescales of diamond growth. *Geochim. Cosmochim. Ac.* **120**, 363-394.

16. Wirth, R., Kaminsky, F., Matsyuk, S. and Schreiber, A., 2009. Unusual micro- and nano-inclusions in diamonds from the Juina area, Brazil. *Earth Planet. Sci. Lett.* **286**, 292-303.

17. Zedgenizov, D.A., Kagi, H., Shatsky, V.S., Ragozin, A.L., 2014. Local variations of carbon isotope composition in diamonds from Sao-Luis (Brazil): evidence for heterogenous carbon reservoir in sublithospheric mantle. *Chem. Geol.* **363**, 114–124.

Figure 1: Depth of formation of Monastery and Jagersfontein diamonds based on the Si-excess in majorite garnets based on experimental data from Wijbrands et al. (2016). The chemical composition data of majorites for Jagersfontein and Monastery diamonds are from Tappert et al. (2005a) and Moore et al. (1991) respectively.

Figure 2: Cathodoluminescence images of diamonds JF50 and Mon B9-07. Transects represent the SIMS analyses of carbon isotopes and nitrogen abundances (dotted lines). The nitrogen isotopes analyses were right beside those points, but not on the same spot as the $\delta^{13}C$ analyses.

Figure 3: Aggregation states (%B) and nitrogen abundances (at.ppm) by Fourier Transform infrared (FTIR) analysis of Monastery (this study) and Jagersfontein diamonds (Tappert et al., 2005a). Isotherms are based on second order kinetics for nitrogen diffusion in diamond (Chrenko et al., 1977, Taylor et al., 1990), and have been calculated for a mantle residence time of 100Ma (Tappert et al., 2005b). Accuracy for both nitrogen aggregation state and N content is generally better than ±5% and 15%, respectively (2σ).

Figure 4: Modelling of the variation between $\delta^{13}C$-$\delta^{15}N$-N for Mon B9-07 following a Rayleigh distillation process. Free parameters such as initial $\delta^{13}C$, $\delta^{15}N$, nitrogen content N/C of the fluid, the partitioning coefficient $K_N$ and the fractionation factors $\Delta$ for C and N between diamond and diamond-forming fluid are varied for calculations to best fit to data points. The core and rim parts of the diamond are indicated. Error bars are 2σ.

Figure 5: Modelling of the variation between $\delta^{13}$C-N for JF09 and JF44 following a Rayleigh distillation process. The parameters and methodology are identical to those reported in the Fig. 4.

Figure 6: Modelling of the variation between $\delta^{13}$C-N for Mon A4-03 and JF58 following a Rayleigh distillation process. The parameters and methodology are identical to those reported in the Fig. 4.

Figure 7: Modelling of the variation between $\delta^{13}$C-$\delta^{15}$N-N for JF50 following a Rayleigh distillation process. The parameters and methodology are identical to those reported in the Fig. 4.

Figure 8: $\delta^{13}$C-$\delta^{15}$N values of Monastery and Jagersfontein diamonds. For comparison the following reservoirs are reported: carbon in carbonates and organic matter (Schidlowski, 1987), carbon and nitrogen in subducted material (i.e. subducted sediments, oceanic crust and lithosphere) (Thomazo et al., 2009, Busigny and Bebout, 2013) and mantle-related material (Cartigny and Marty, 2013). Also shown are the carbon and nitrogen isotopic composition of diamonds from the lithosphere, the asthenosphere/transition zone and the lower mantle from Sao Luiz (Hutchinson et al., 1999; Palot et al., 2012) and Kankan (Palot et al., 2012, 2014), the two main localities providing ultra-deep diamonds. Error bars are 2 σ.

Figure 9 Chondrite-normalized (McDonough and Sun, 1995) rare earth element compositions of majoritic garnet inclusions in diamond from Monastery (Moore et al., 1991) and Jagersfontein (Tappert et al., 2005a, b).

Figure 10 Carbon isotope fractionation factors derived for the studied diamonds and for possible C-species in the fluid, where $\Delta C_{diamond\text{-}fluid} = 1000 \ln \alpha_{diamond\text{-}species}$. Shown are diamond-$Fe_3C$, diamond-$CH_4$, diamond-$CaCO_3$ and diamond-$CO_2$ fractionation curves which represent the main possible C-bearing phases involved in the formation diamonds. The curves are derived from theoretical calculations or laboratory and empirical measurements (Bottinga, 1969, Richet et al., 1977, Chacko et al., 1991, 2001, Polyakov and Kharlashina, 1995, Satish-Kumar et al., 2011), but data are mostly lacking at high temperatures (>1000°C) and are extrapolated here.

Figure 11 Nitrogen isotope fractionation factors for diamond Mon B9-07 and possible N-species in the fluid. Fractionation curves of $CN^-$–$N_2$, $CN^-$–$NH_3$ and $CN^-$–$NH_4^+$ are reported as the best possible analogue for the diamond-fluid system. This figure has been modified from Fig. 6 in Petts et al., 2015 and the reader is referred to this study and references therein for detailed discussion and data sources. Also included is the empirical fractionation factor (calculated from C- and N-isotope analyses) for lithospheric diamond JDE-25 from Jericho, Canada (Petts et al., 2015), lithospheric diamonds from Premier, RSA (Thomassot et al., 2007) and sublithospheric diamonds KK-200 and KK-204 from Kankan, Guinea (Palot et al., 2014).

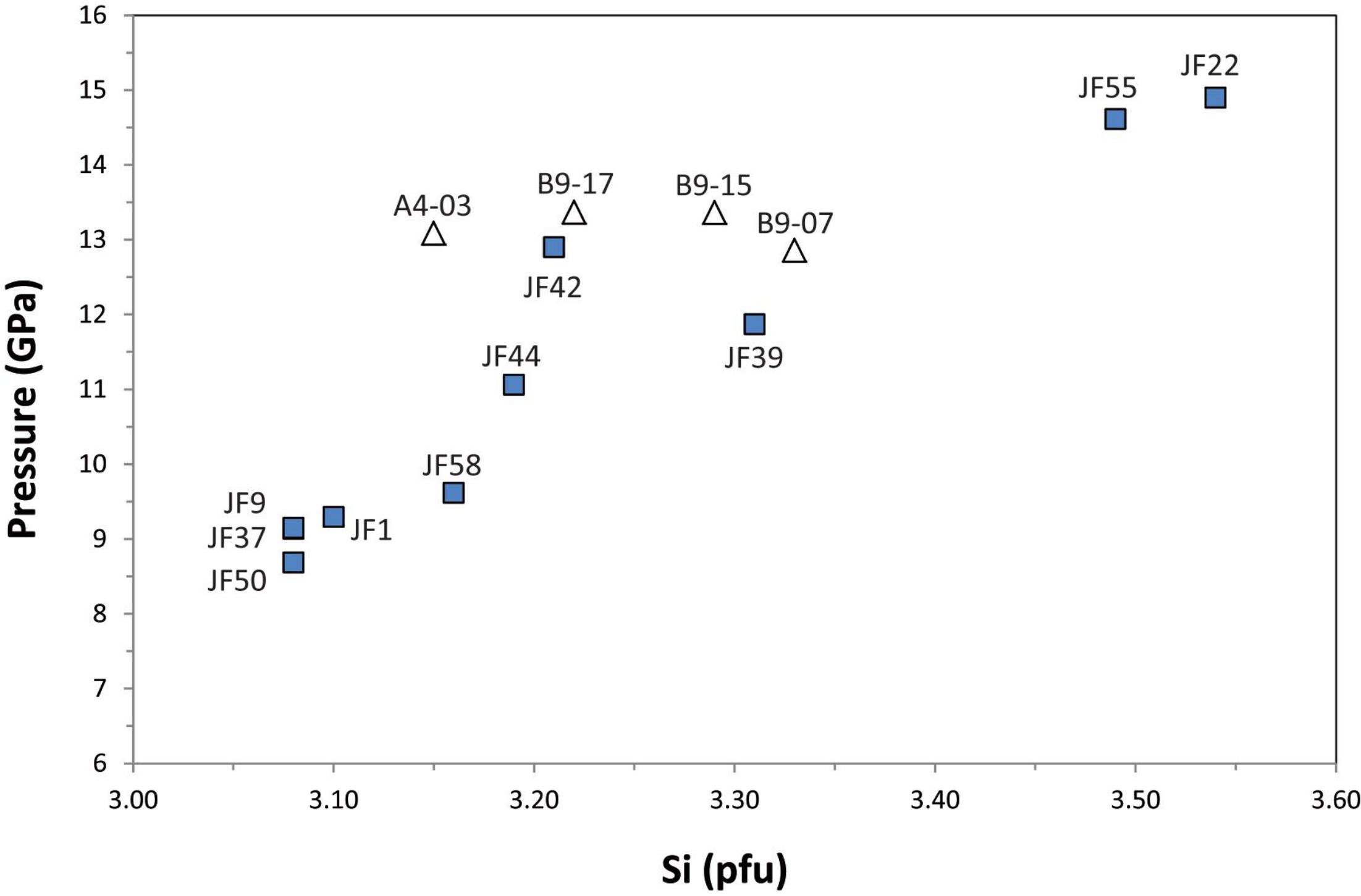
Pressure (GPa)
16
15
14
13
12
11
10
9
8
7
6
3.00
3.10
3.20
3.30
3.40
3.50
3.60
Si (pfu)
JF22
JF55
B9-17
B9-15
A4-03
B9-07
JF42
JF44
JF39
JF58
JF9
JF37
JF1
JF50

a)

JF50

Rim

Core

Transect 1

Transect 2

1 2 3 4 5 6 7 8 9 10 11 12 13 14 15 17

200 µm

b)

Mon B9-07

Rim

Core

Transect 1

Transect 2

Transect 3

1 2 3 4 5 6 7 8 9 10 11 12 13 14 15 16 17 18 19 20 21 22 23

100 µm

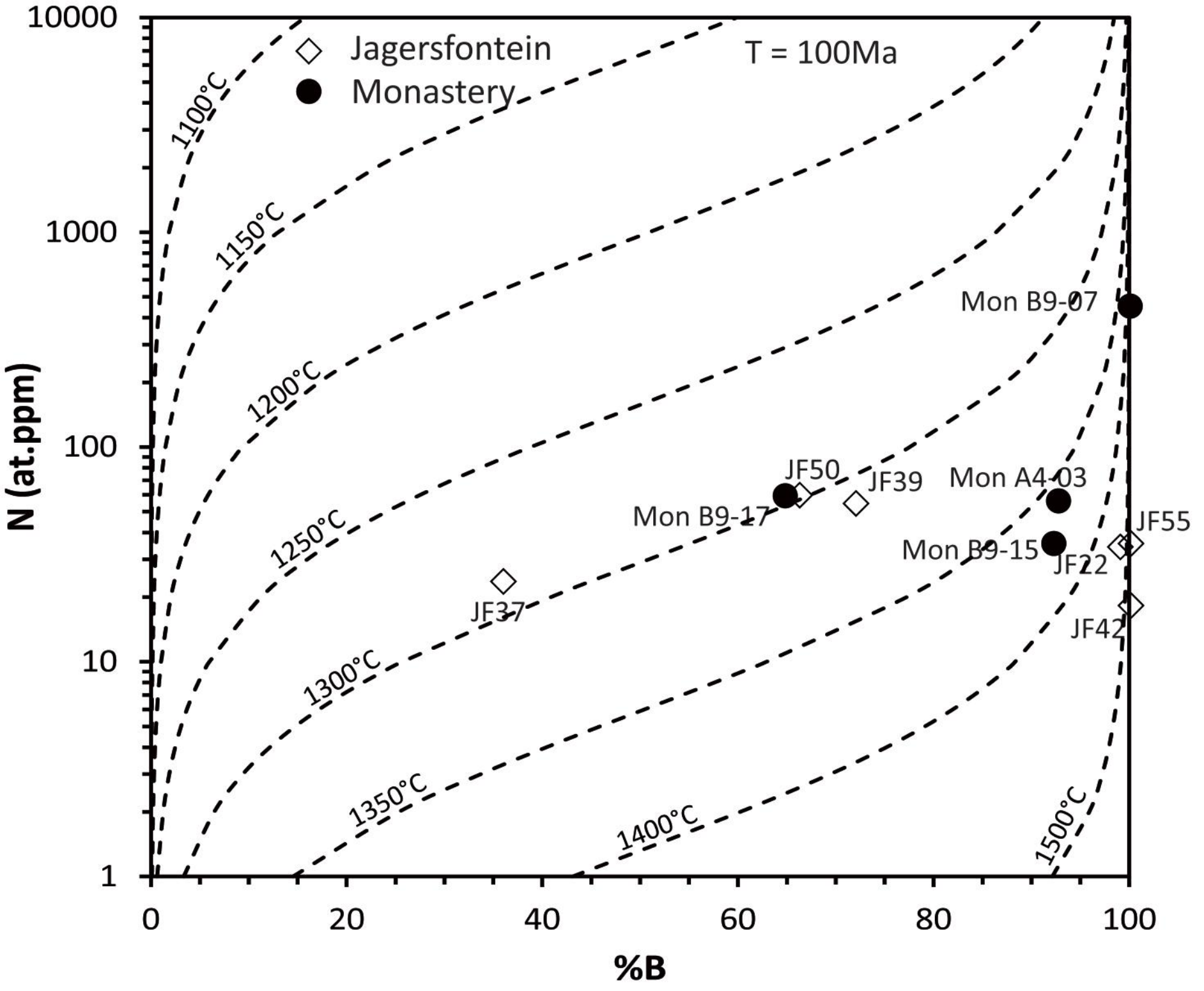
Jagersfontein
Monastery
T = 100Ma
1100°C
1150°C
1200°C
1250°C
1300°C
1350°C
1400°C
1500°C
Mon B9-07
JF50
JF39
Mon A4-03
Mon B9-17
JF55
Mon B9-15
JF22
JF37
JF42
10000
1000
100
10
1
N (at.ppm)
0
20
40
60
80
100
%B

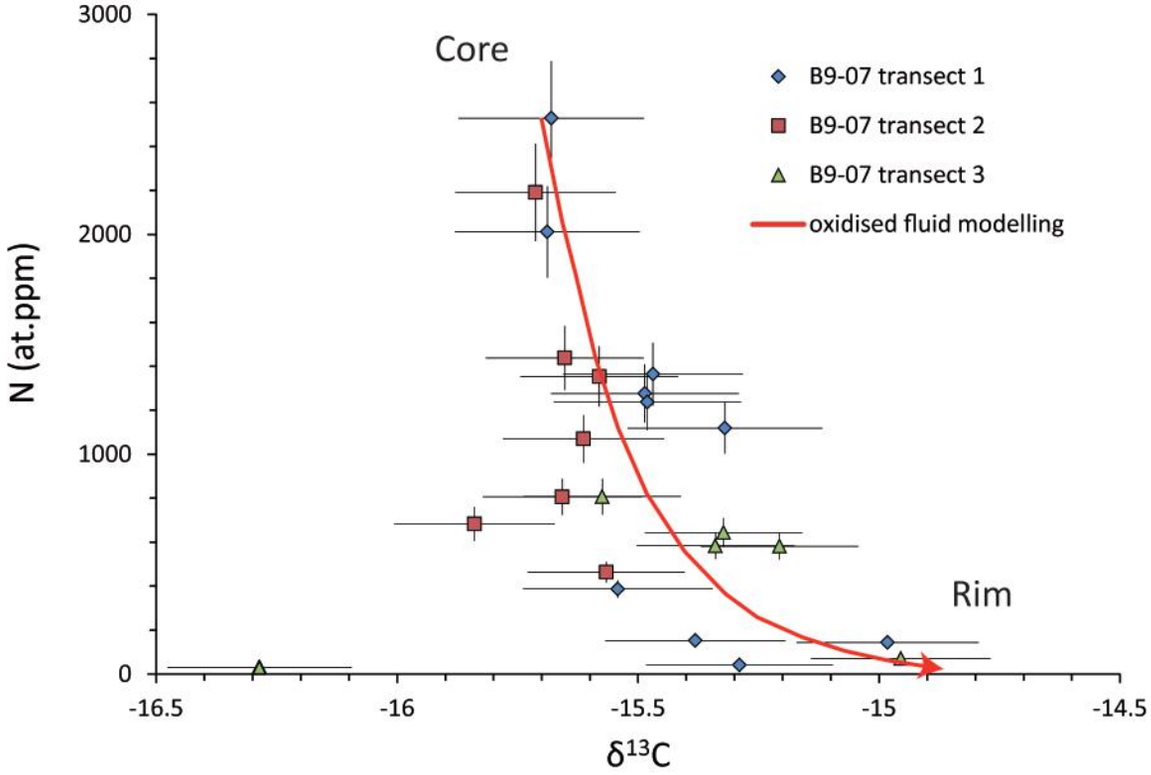
Core
B9-07 transect 1
B9-07 transect 2
B9-07 transect 3
oxidised fluid modelling
Rim
N (at.ppm)
3000
2000
1000
0
-16.5
-16
-15.5
-15
-14.5
δ13C

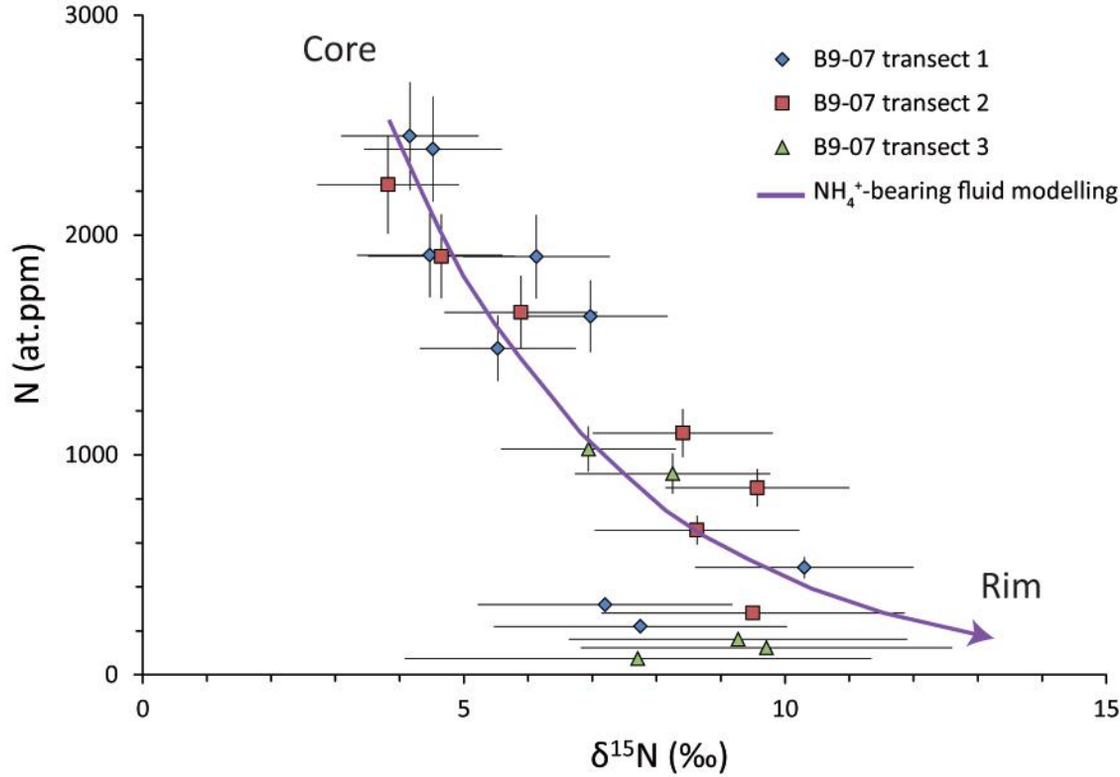
Core
B9-07 transect 1
B9-07 transect 2
B9-07 transect 3
NH4+-bearing fluid modelling
Rim
N (at.ppm)
3000
2000
1000
0
0
5
10
15
δ15N (‰)

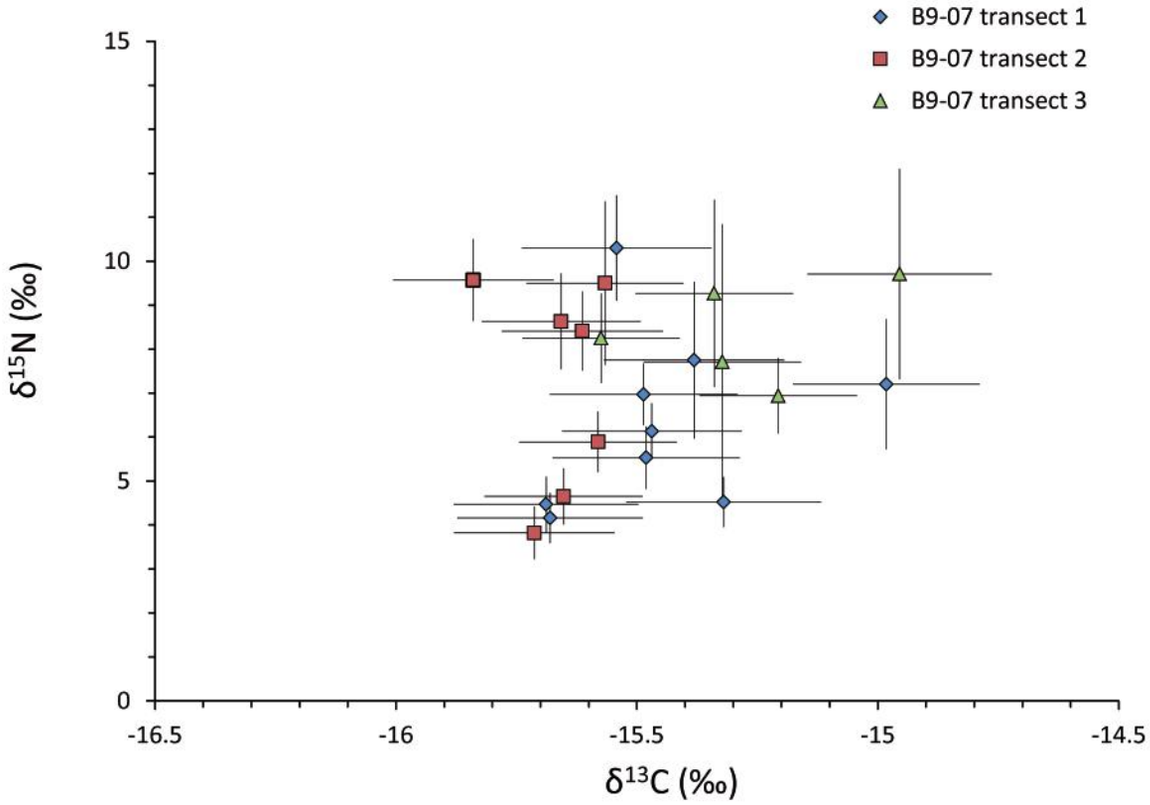
B9-07 transect 1
B9-07 transect 2
B9-07 transect 3
δ15N (‰)
15
10
5
0
-16.5
-16
-15.5
-15
-14.5
δ13C (‰)

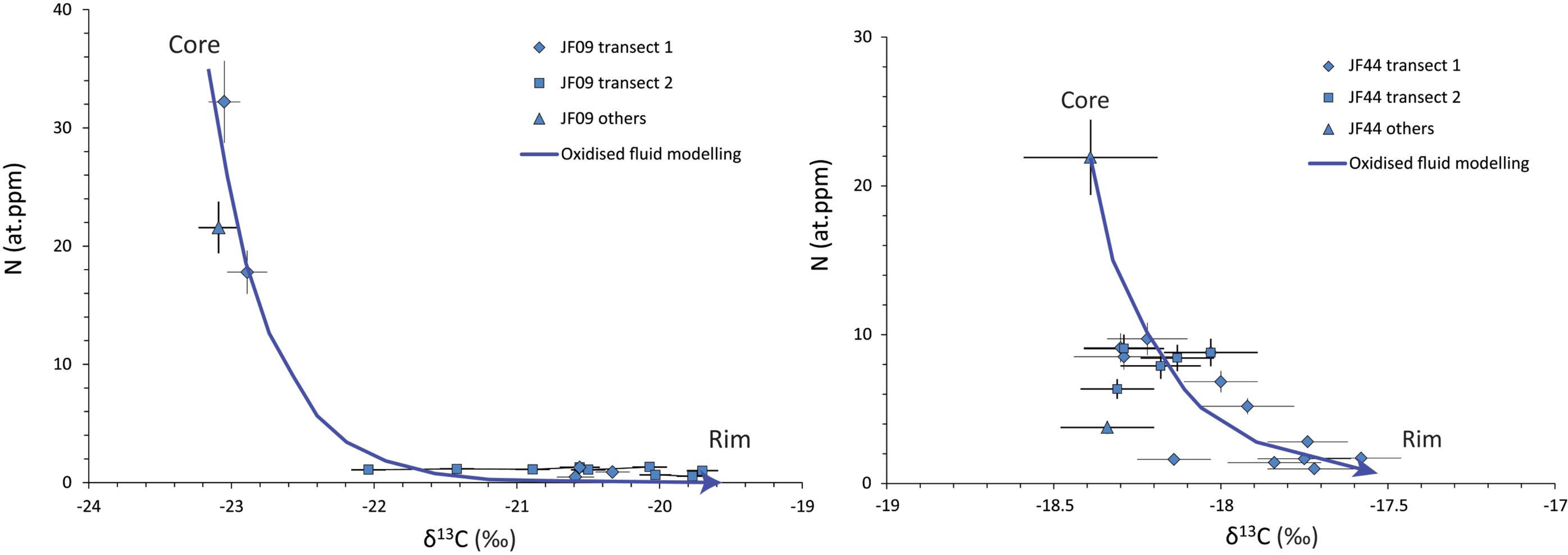
Core
Rim
JF09 transect 1
JF09 transect 2
JF09 others
Oxidised fluid modelling
N (at.ppm)
δ13C (‰)
40
30
20
10
0
-24
-23
-22
-21
-20
-19
Core
Rim
JF44 transect 1
JF44 transect 2
JF44 others
Oxidised fluid modelling
N (at.ppm)
δ13C (‰)
30
20
10
0
-19
-18.5
-18
-17.5
-17

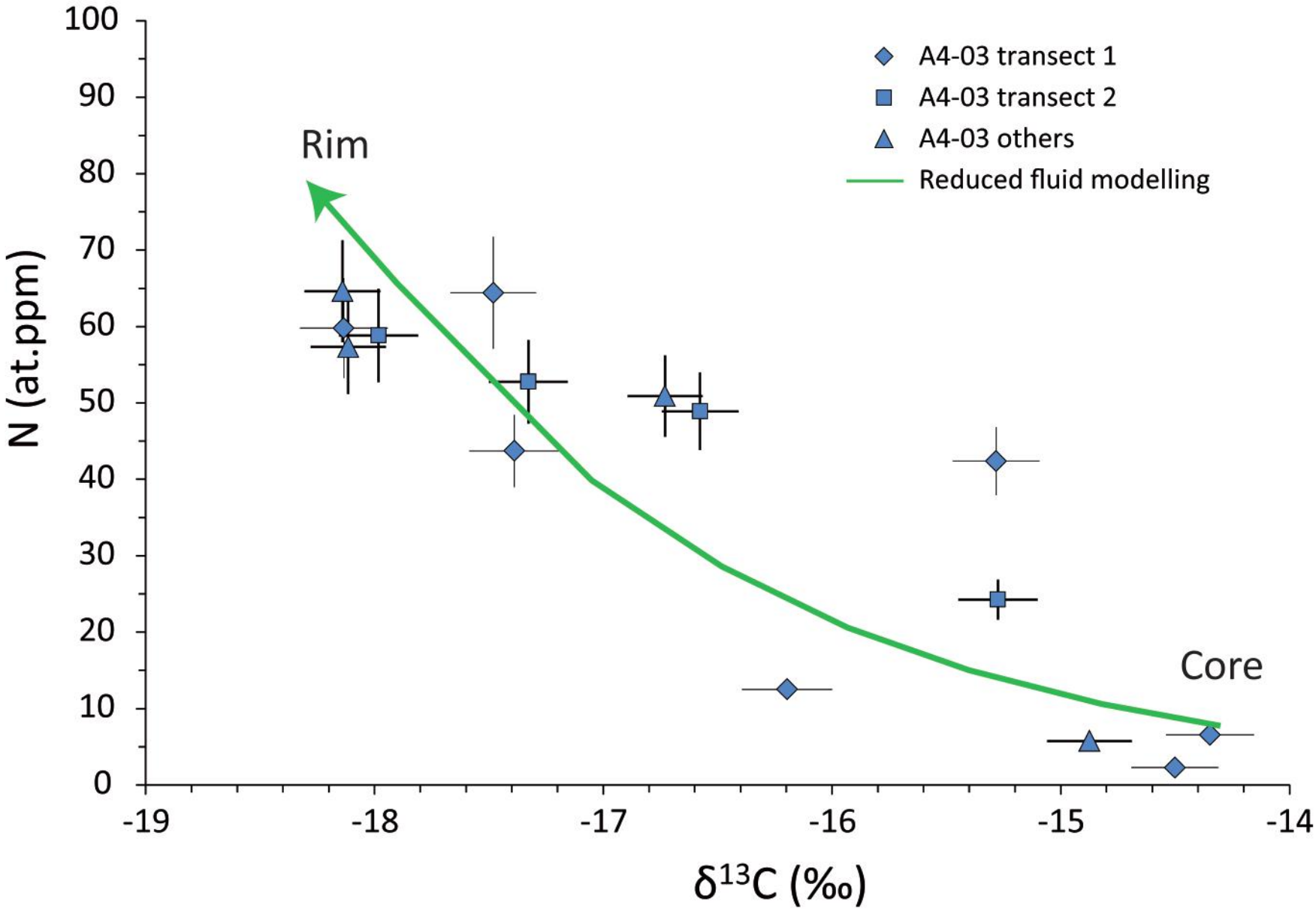
A4-03 transect 1
A4-03 transect 2
A4-03 others
Reduced fluid modelling
Rim
Core
N (at.ppm)
δ13C (‰)
100
90
80
70
60
50
40
30
20
10
0
-19
-18
-17
-16
-15
-14


Outer zones
Inner zone
JF58 transect 1
JF58 others
Reduced fluid modelling
N (at.ppm)
δ13C (‰)
100
80
60
40
20
0
-22
-21.5
-21
-20.5
-20
-19.5
-19

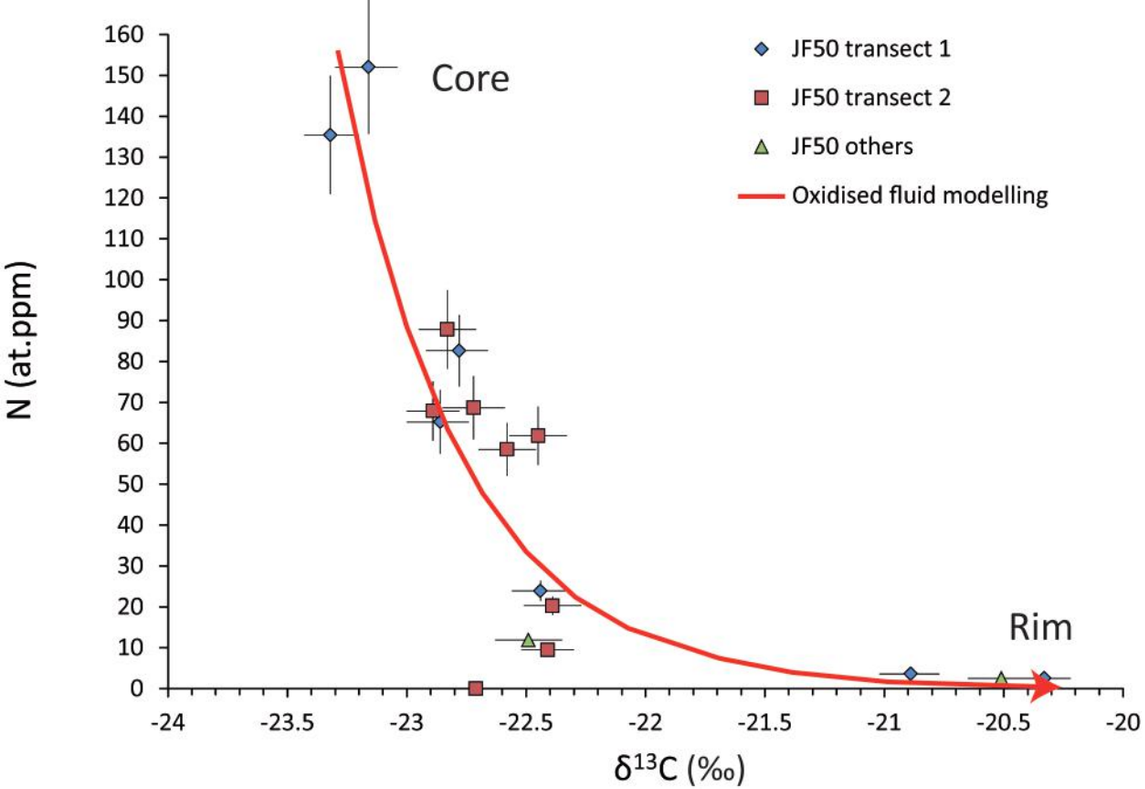
Core
Rim
JF50 transect 1
JF50 transect 2
JF50 others
Oxidised fluid modelling
N (at.ppm)
δ13C (‰)

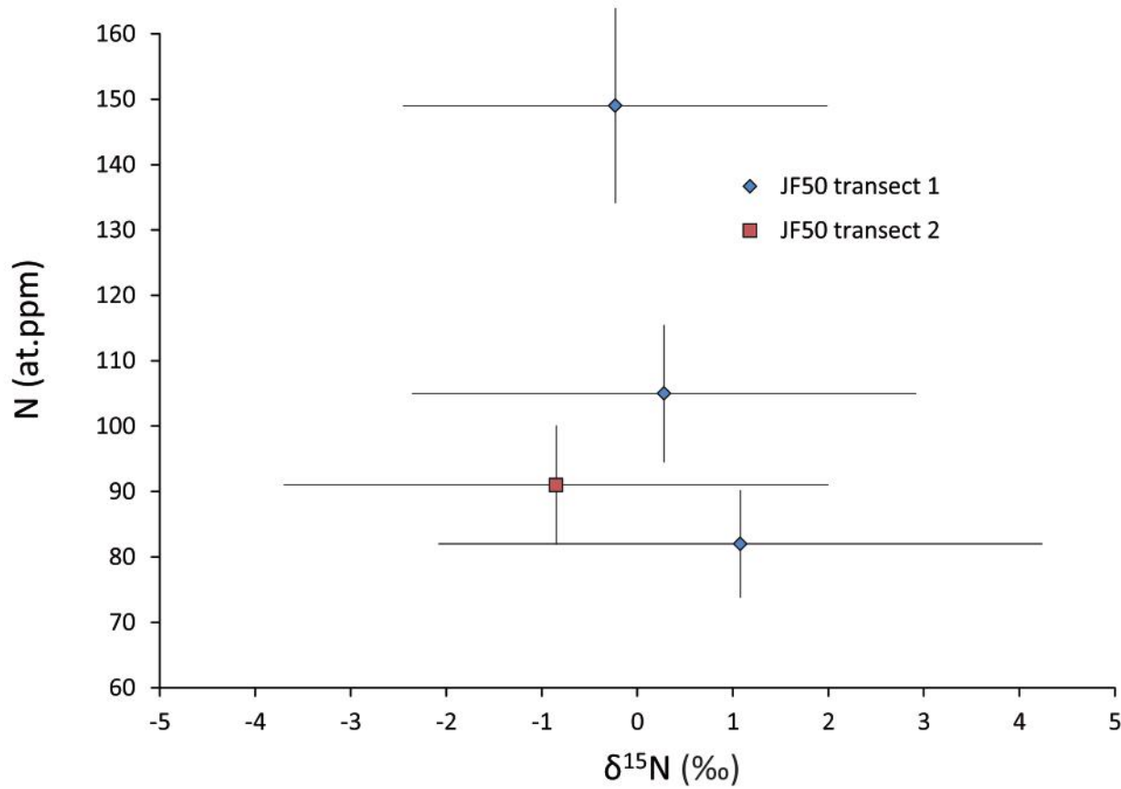
JF50 transect 1
JF50 transect 2
N (at.ppm)
δ15N (‰)

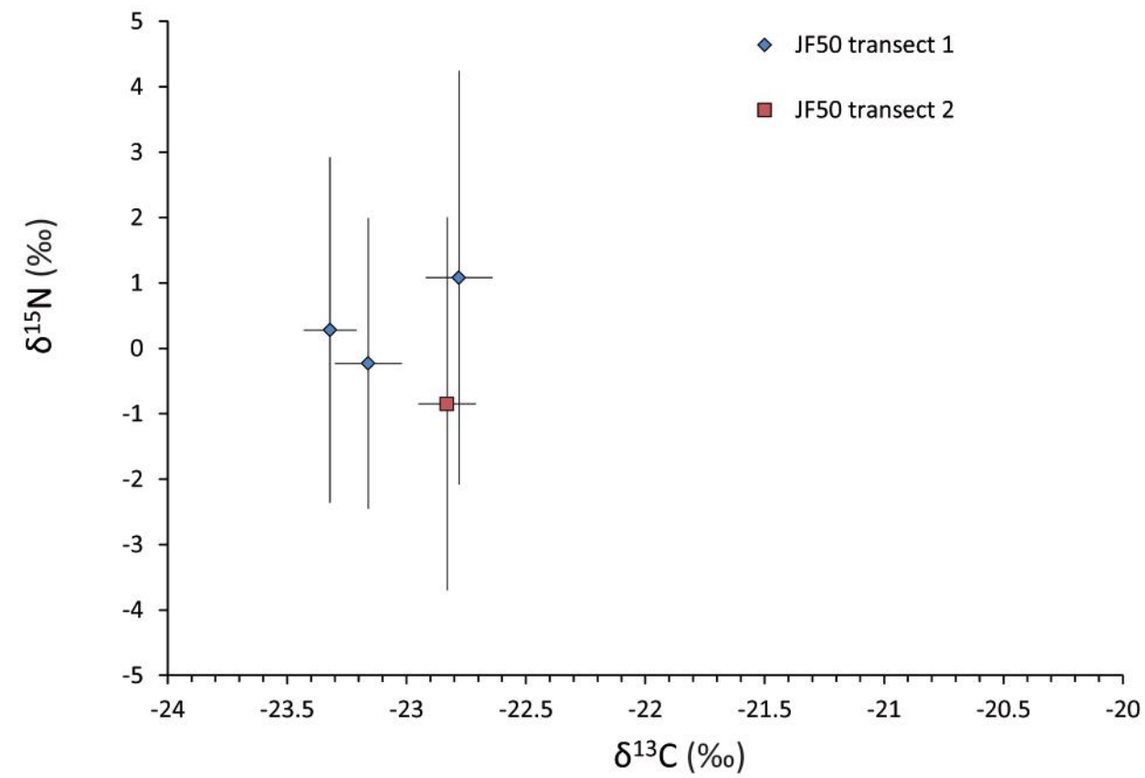
JF50 transect 1
JF50 transect 2
δ15N (‰)
δ13C (‰)

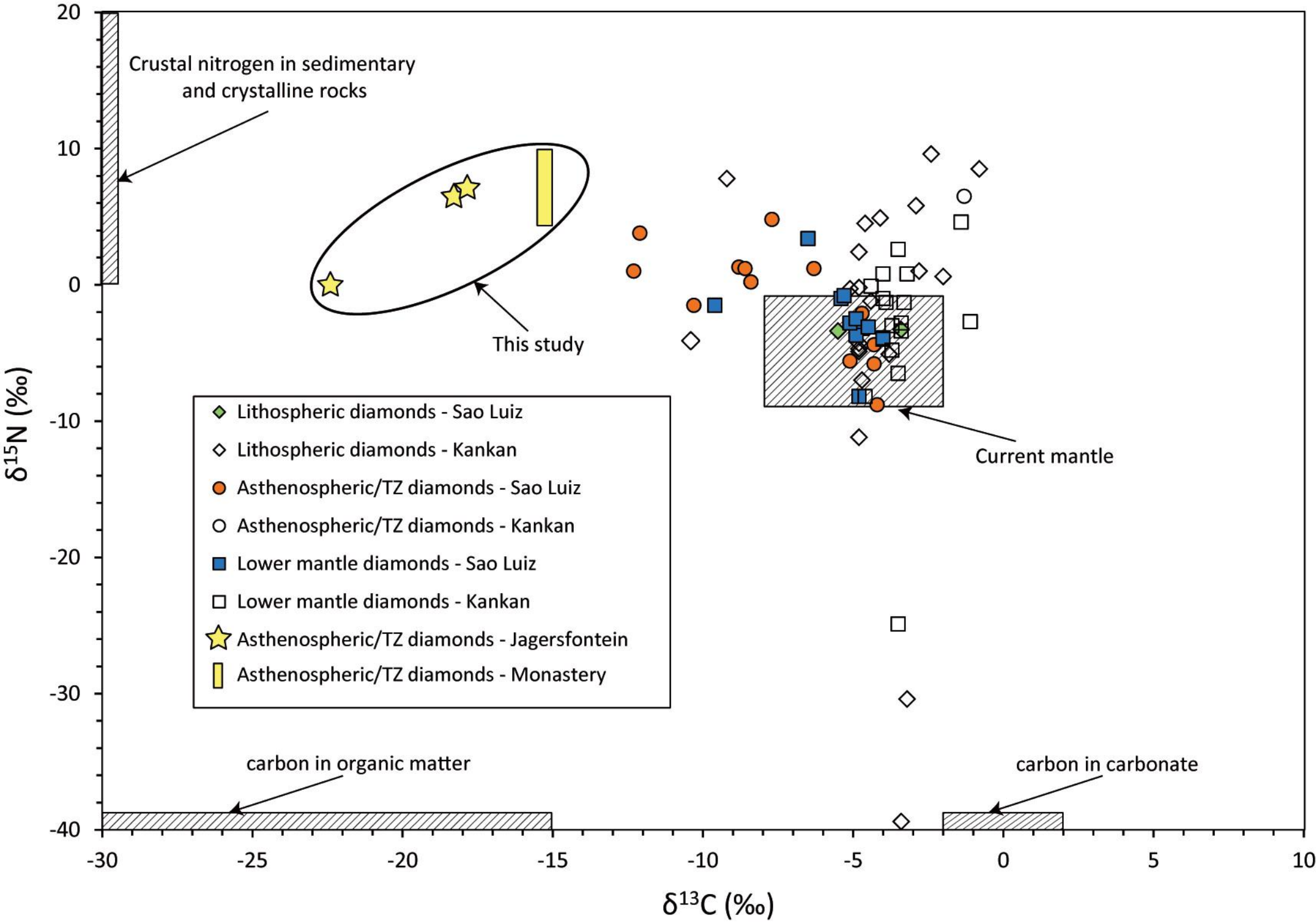
Crustal nitrogen in sedimentary and crystalline rocks
This study
Current mantle
carbon in organic matter
carbon in carbonate
Lithospheric diamonds - Sao Luiz
Lithospheric diamonds - Kankan
Asthenospheric/TZ diamonds - Sao Luiz
Asthenospheric/TZ diamonds - Kankan
Lower mantle diamonds - Sao Luiz
Lower mantle diamonds - Kankan
Asthenospheric/TZ diamonds - Jagersfontein
Asthenospheric/TZ diamonds - Monastery
δ15N (‰)
δ13C (‰)
20
10
0
-10
-20
-30
-40
-30
-25
-20
-15
-10
-5
0
5
10

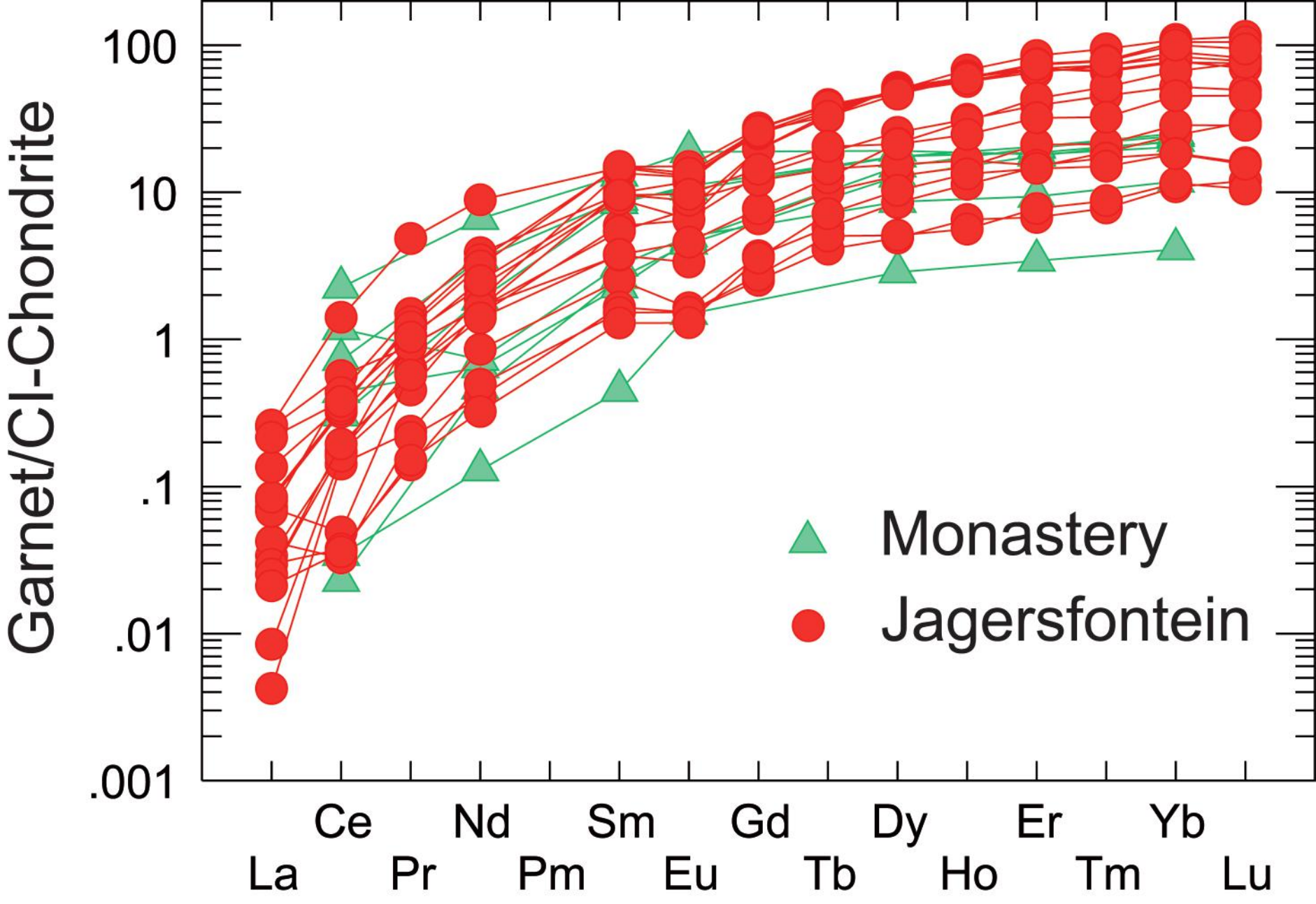
Garnet/CI-Chondrite
100
10
1
.1
.01
.001
Monastery
Jagersfontein
La
Ce
Pr
Nd
Pm
Sm
Eu
Gd
Tb
Dy
Ho
Er
Tm
Yb
Lu

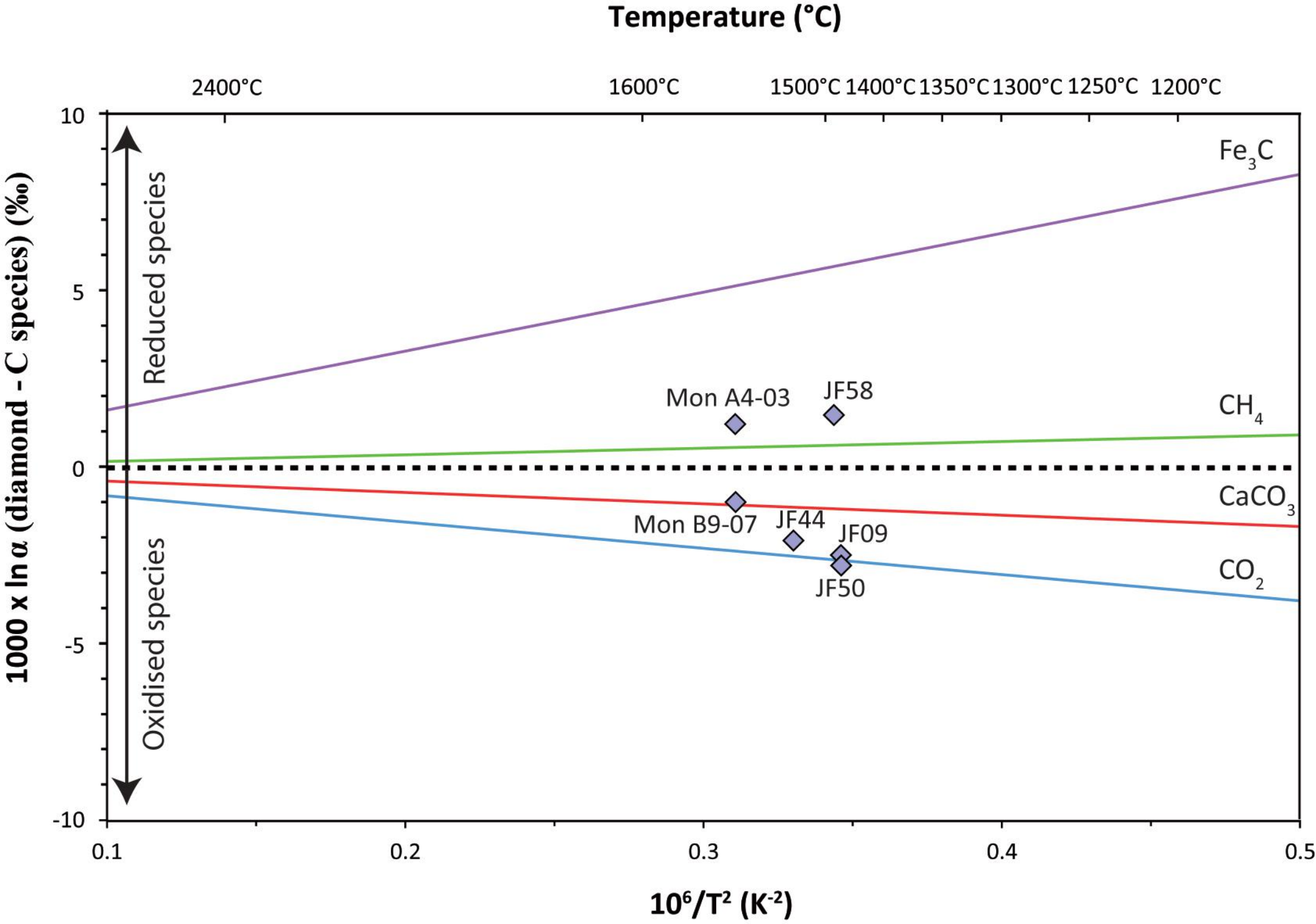
Temperature (°C)
2400°C
1600°C
1500°C
1400°C
1350°C
1300°C
1250°C
1200°C
10
5
0
-5
-10
1000 x ln α (diamond - C species) (‰)
Reduced species
Oxidised species
Fe3C
CH4
CaCO3
CO2
Mon A4-03
JF58
Mon B9-07
JF44
JF09
JF50
0.1
0.2
0.3
0.4
0.5
10⁶/T² (K⁻²)

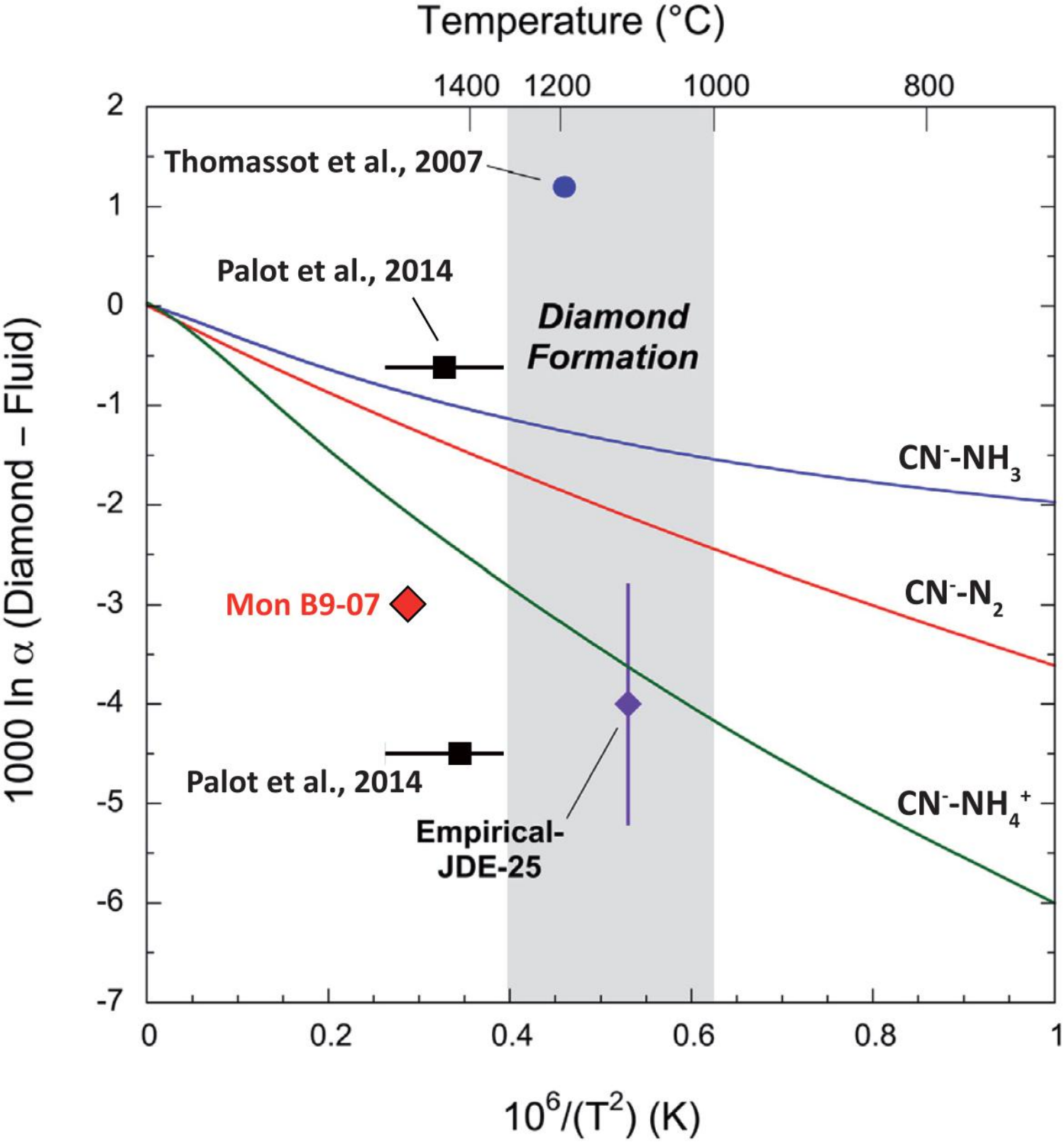
Temperature (°C)
1400
1200
1000
800
2
1
0
-1
-2
-3
-4
-5
-6
-7
1000 ln α (Diamond – Fluid)
Thomassot et al., 2007
Palot et al., 2014
Diamond Formation
CN⁻-NH3
CN⁻-N2
Mon B9-07
Palot et al., 2014
Empirical-JDE-25
CN⁻-NH4⁺
0
0.2
0.4
0.6
0.8
1
10⁶/(T²) (K)

Table 1: Paragenesis of the Jagersfontein and Monastery diamonds and depth of formation (Moore and Gurney, 1985; Moore et al., 1991; Tappert et al., 2005a, 2005b). $T_{inclusion}$ are estimates based on majorite inclusion barometry (see Fig. 1) projected on the mantle adiabat of Katsura et al., (2010). $T_{N\text{-}aggregation}$ represent the average nitrogen aggregation temperatures in diamonds, calculated for a mantle residence time of 100Ma (Tappert et al., 2005). N.d. = non determined because of the lack of accuracy either for very low nitrogen level samples or fully aggregated diamonds. Estimated accuracy ±20°C (1σ).

| **Sample name** | **Locality** | **Inclusions** | **Paragenese** | **Approximative Depth (km)**[a] | **$T_{inclusion}$** (°C) | **$T_{N\text{-}agg.}$** (°C) | **$\Delta T_{inclusion}$-$T_{N\text{-}agg}$** (°C) |
|---|---|---|---|---|---|---|---|
| **JF01** | Jagersfontein | Maj Garnet | Eclogitic | 260 | 1490 | n.d. | |
| **JF09** | Jagersfontein | Maj Garnet | Eclogitic | 256 | 1480 | n.d. | |
| **JF22** | Jagersfontein | Maj Garnet | Eclogitic | 413 | 1580 | 1480 | 100 |
| **JF37** | Jagersfontein | Maj Garnet | Eclogitic | 256 | 1480 | 1280 | 200 |
| **JF39** | Jagersfontein | Maj Garnet | Eclogitic | 330 | 1530 | 1315 | 215 |
| **JF42** | Jagersfontein | Maj Garnet | Eclogitic | 358 | 1550 | n.d. | |
| **JF43** | Jagersfontein | Maj Garnet | Websteritic | 325? | | | |
| **JF44** | Jagersfontein | Maj Garnet | Eclogitic | 308 | 1520 | n.d. | |
| **JF50** | Jagersfontein | Maj Garnet | Eclogitic | 244 | 1480 | 1300 | 280 |
| **JF55** | Jagersfontein | Maj Garnet | Eclogitic | 405 | 1580 | n.d. | |
| **JF58** | Jagersfontein | Maj Garnet | Eclogitic | 269 | 1490 | n.d. | |
| **Mon A4-03** | Monastery | Maj Garnet | Eclogitic | 363 | 1550 | 1360 | 190 |
| **Mon B9-07** | Monastery | Maj Garnet | Eclogitic | 357 | 1550 | n.d. | |
| **Mon B9-15** | Monastery | Maj Garnet | Eclogitic | 371 | 1560 | 1375 | 185 |
| **Mon B9-17** | Monastery | Maj Garnet | Eclogitic | 371 | 1560 | 1300 | 260 |

[a] Estimated from the majorite barometer of Wijbrans et al. (2016).

Table 2: Carbon and nitrogen isotope and nitrogen abundance data of Monastery diamonds

| Diamond | Reference number on CL images | $\delta^{13}C$ (VDP) | 2σ (‰) | [N] at.ppm[a] | 2σ | $\delta^{15}N$ (air) | 2σ (‰) | [N] at.ppm[b] | 2σ |
|---|---|---|---|---|---|---|---|---|---|
| | | | | Transect 1 | | | | | |
| Mon A4-03 | 1 | -17.4 | 0.1 | 44 | 5 | | | | |
| Mon A4-03 | 2 | -17.5 | 0.1 | 64 | 7 | | | | |
| Mon A4-03 | 3 | -16.7 | 0.1 | 51 | 5 | | | | |
| Mon A4-03 | 4 | -18.1 | 0.1 | 60 | 6 | | | | |
| Mon A4-03 | 5 | -16.6 | 0.1 | 49 | 5 | | | | |
| Mon A4-03 | 6 | -15.3 | 0.1 | 42 | 4 | | | | |
| Mon A4-03 | 7 | -14.5 | 0.1 | 2 | 0 | | | | |
| | | | | Transect 2 | | | | | |
| Mon A4-03 | 12 | -17.3 | 0.1 | 53 | 5 | | | | |
| Mon A4-03 | 13 | -17.9 | 0.1 | 59 | 6 | | | | |
| Mon A4-03 | 14 | -18.1 | 0.1 | 57 | 6 | | | | |
| Mon A4-03 | 15 | -18.1 | 0.1 | 65 | 7 | | | | |
| | | | | Others | | | | | |
| Mon A4-03 | 8 | -14.3 | 0.1 | 7 | 1 | | | | |
| Mon A4-03 | 9 | -16.2 | 0.1 | 12 | 1 | | | | |
| Mon A4-03 | 10 | -14.9 | 0.1 | 5.7 | 1 | | | | |
| | | | | Transect 1 | | | | | |
| Mon B9-07 | 1 | -14.9 | 0.1 | 143 | 15 | 7.2 | 1.5 | 319 | 32 |
| Mon B9-07 | 2 | -15.3 | 0.1 | 42 | 4 | | | | |
| Mon B9-07 | 3 | -15.5 | 0.1 | 387 | 40 | 10.3 | 1.2 | 488 | 49 |
| Mon B9-07 | 4 | -15.7 | 0.1 | 2528 | 259 | 4.2 | 0.6 | 2451 | 245 |
| Mon B9-07 | 5 | -15.5 | 0.1 | 1237 | 128 | 5.5 | 0.7 | 1485 | 148 |
| Mon B9-07 | 6 | -15.5 | 0.1 | 1276 | 131 | 7.0 | 0.7 | 1631 | 163 |
| Mon B9-07 | 7 | -15.3 | 0.1 | 1119 | 116 | 4.5 | 0.6 | 2391 | 239 |
| Mon B9-07 | 8 | -15.7 | 0.1 | 2011 | 207 | 4.5 | 0.6 | 1909 | 191 |
| Mon B9-07 | 9 | -15.4 | 0.1 | 153 | 16 | 7.7 | 1.8 | 220 | 22 |
| Mon B9-07 | 10 | -15.5 | 0.1 | 1364 | 143 | 6.1 | 0.6 | 1902 | 190 |
| | | | | Transect 2 | | | | | |
| Mon B9-07 | 16 | -15.7 | 0.1 | 806 | 82 | 8.6 | 1.1 | 658 | 66 |
| Mon B9-07 | 15 | -15.8 | 0.1 | 683 | 77 | 9.6 | 0.9 | 851 | 85 |
| Mon B9-07 | 14 | -15.6 | 0.1 | 1438 | 145 | 4.6 | 0.6 | 1904 | 190 |
| Mon B9-07 | 13 | -15.6 | 0.1 | 1070 | 108 | 8.4 | 0.9 | 1100 | 110 |
| Mon B9-07 | 12 | -15.6 | 0.1 | 1353 | 137 | 5.9 | 0.7 | 1649 | 165 |
| Mon B9-07 | 11 | -15.7 | 0.1 | 2190 | 221 | 3.8 | 0.6 | 2229 | 223 |
| | | | | Transect 3 | | | | | |
| Mon B9-07 | 18 | -15.3 | 0.1 | 644 | 66 | 7.7 | 3.1 | 74 | 7 |
| Mon B9-07 | 19 | -15.2 | 0.1 | 581 | 59 | 6.9 | 0.9 | 1027 | 103 |
| Mon B9-07 | 20 | -15.6 | 0.1 | 807 | 82 | 8.2 | 1.0 | 915 | 91 |
| Mon B9-07 | 21 | -15.3 | 0.1 | 583 | 60 | 9.3 | 2.1 | 162 | 16 |
| Mon B9-07 | 22 | -14.9 | 0.1 | 70 | 8 | 9.7 | 2.4 | 123 | 12 |
| | | | | Others | | | | | |
| Mon B9-07 | 17 | -15.6 | 0.1 | 463 | 47 | 9.5 | 1.9 | 281 | 28 |
| Mon B9-07 | 23 | -16.3 | 0.1 | 30 | 3 | | | | |
| | | | | Transect 1 | | | | | |
| Mon B9-15 | 1 | -18.4 | 0.1 | 27 | 3 | | | | |
| Mon B9-15 | 2 | -18.2 | 0.1 | 16 | 2 | | | | |
| Mon B9-15 | 3 | -18.3 | 0.1 | 17 | 2 | | | | |
| Mon B9-15 | 4 | -18.4 | 0.1 | 22 | 2 | | | | |
| Mon B9-15 | 5 | -18.2 | 0.1 | 6 | 1 | | | | |
| | | | | Others | | | | | |
| Mon B9-15 | 8 | -18.7 | 0.1 | 34 | 4 | | | | |

| | | | | | |
|---|---|---|---|---|---|
| Mon B9-15 | 7 | -18.4 | 0.1 | 33 | 3 |
| Mon B9-15 | 6 | -18.2 | 0.1 | 31 | 3 |
| | | | | Transect 1 | |
| Mon B9-17 | 1 | -17.4 | 0.1 | 40 | 4 |
| Mon B9-17 | 2 | -17.3 | 0.1 | 18 | 2 |
| Mon B9-17 | 4 | -16.5 | 0.1 | 36 | 4 |
| Mon B9-17 | 6 | -16.3 | 0.1 | 8 | 1 |
| Mon B9-17 | 7 | -16.8 | 0.1 | 27 | 3 |
| Mon B9-17 | 8 | -15.7 | 0.1 | 28 | 3 |
| Mon B9-17 | 9 | -15.6 | 0.1 | 27 | 3 |
| Mon B9-17 | 10 | -15.6 | 0.1 | 28 | 3 |
| | | | | Others | |
| Mon B9-17 | 3 | -16.8 | 0.1 | 21 | 2 |
| Mon B9-17 | 5 | -15.7 | 0.1 | 2 | 0 |
| Mon B9-17 | 11 | -15.7 | 0.1 | 26 | 3 |

[a] Measured with carbon isotopic analyses.
[b] Measured with nitrogen isotopic analyses.

Table 3: Carbon and nitrogen isotope and nitrogen abundance data of Jagersfontein diamonds

| Diamond | Reference number on CL images | $\delta^{13}C$ (VDP) | 2σ (‰) | [N] at.ppm[a] | 2σ | $\delta^{15}N$ (air) | 2σ (‰) | [N] at.ppm[b] | 2σ |
|---|---|---|---|---|---|---|---|---|---|
| | | | | Transect 1 | | | | | |
| JF01 | 1 | -21.6 | 0.2 | 6 | 1 | | | | |
| JF01 | 2 | -21.9 | 0.1 | 16 | 2 | | | | |
| JF01 | 3 | -21.6 | 0.1 | 13 | 1 | | | | |
| JF01 | 4 | -21.1 | 0.1 | 17 | 2 | | | | |
| JF01 | 5 | -25.3 | 0.1 | 5 | 1 | | | | |
| JF01 | 6 | -23.3 | 0.1 | 2 | 0 | | | | |
| JF01 | 7 | -23.2 | 0.1 | 2 | 0 | | | | |
| JF01 | 8 | -23.4 | 0.1 | | | | | | |
| JF01 | 9 | -23.4 | 0.1 | 1 | 0 | | | | |
| | | | | Transect 2 | | | | | |
| JF01 | 10 | -23.6 | 0.1 | 4 | 0 | | | | |
| JF01 | 11 | -23.3 | 0.1 | 4 | 0 | | | | |
| JF01 | 12 | -23.3 | 0.1 | 2 | 0 | | | | |
| JF01 | 7 | -23.2 | 0.1 | 2 | 0 | | | | |
| JF01 | 13 | -23.3 | 0.1 | 2 | 0 | | | | |
| JF01 | 14 | -21.4 | 0.1 | 7 | 1 | | | | |
| JF01 | 15 | -25.7 | 0.1 | | | | | | |
| JF01 | 16 | -21.3 | 0.1 | 29 | 3 | | | | |
| | | | | Others | | | | | |
| JF01 | 19 | -25.4 | 0.1 | 4 | 0 | | | | |
| JF01 | 18 | -21.5 | 0.1 | 2 | 0 | | | | |
| JF01 | 17 | -21.3 | 0.1 | 7 | 1 | | | | |
| Transect 1 | | | | | | | | | |
| JF09 | 5 | -20.6 | 0.1 | 1 | 0 | | | | |
| JF09 | 10 | -20.6 | 0.1 | 0 | 0 | | | | |
| JF09 | 11 | -20.3 | 0.1 | 1 | 0 | | | | |
| JF09 | 12 | -22.9 | 0.1 | 18 | 2 | | | | |
| JF09 | 13 | -23.1 | 0.1 | 32 | 3 | | | | |
| Transect 2 | | | | | | | | | |
| JF09 | 9 | -22.0 | 0.1 | 1 | 0 | | | | |
| JF09 | 8 | -21.4 | 0.1 | 1 | 0 | | | | |
| JF09 | 7 | -20.9 | 0.1 | 1 | 0 | | | | |
| JF09 | 6 | -20.6 | 0.1 | 1 | 0 | | | | |
| JF09 | 5 | -20.5 | 0.1 | 1 | 0 | | | | |
| JF09 | 4 | -20.1 | 0.1 | 1 | 0 | | | | |
| JF09 | 3 | -20.0 | 0.1 | 1 | 0 | | | | |
| JF09 | 2 | -19.8 | 0.1 | 1 | 0 | | | | |
| JF09 | 1 | -19.7 | 0.1 | 1 | 0 | | | | |
| Others | | | | | | | | | |
| JF09 | 14 | -23.1 | 0.1 | 22 | 2 | | | | |
| | | | | No CL image | | | | | |
| JF22 | 1 | -18.0 | 0.1 | 32 | 3 | | | | |
| JF22 | 2 | -17.6 | 0.1 | 31 | 3 | | | | |
| JF22 | 3 | -17.5 | 0.1 | 11 | 1 | | | | |
| JF22 | 4 | -17.4 | 0.1 | 10 | 1 | | | | |
| JF22 | 5 | -17.4 | 0.2 | 45 | 5 | | | | |
| JF22 | 6 | -17.5 | 0.1 | 46 | 5 | | | | |
| JF22 | 7 | -17.6 | 0.1 | 50 | 5 | | | | |
| JF22 | 8 | -17.4 | 0.2 | 18 | 2 | | | | |

| | | | | | | | | | |
|---|---|---|---|---|---|---|---|---|---|
| | | | | Transect 1 | | | | | |
| JF37 | 1 | -21.9 | 0.1 | 60 | 6 | | | | |
| JF37 | 2 | -19.7 | 0.1 | 7 | 1 | | | | |
| JF37 | 3 | -22.9 | 0.1 | 11 | 1 | | | | |
| JF37 | 4 | -22.7 | 0.1 | 16 | 2 | | | | |
| JF37 | 5 | -22.6 | 0.1 | 16 | 2 | | | | |
| JF37 | 6 | -22.7 | 0.1 | 19 | 2 | | | | |
| JF37 | 7 | -22.5 | 0.1 | 30 | 3 | | | | |
| JF37 | 8 | -22.7 | 0.1 | 15 | 2 | | | | |
| | | | | | | | | | |
| JF37 | 14 | -22.6 | 0.1 | 17 | 2 | | | | |
| JF37 | 13 | -22.6 | 0.1 | 17 | 2 | | | | |
| JF37 | 12 | -22.7 | 0.1 | 16 | 2 | | | | |
| JF37 | 6 | -22.7 | 0.1 | 19 | 2 | | | | |
| JF37 | 11 | -22.8 | 0.1 | 18 | 2 | | | | |
| JF37 | 10 | -22.9 | 0.1 | 9 | 1 | | | | |
| JF37 | 9 | -22.8 | 0.1 | 5 | 1 | | | | |
| | | | | | | | | | |
| JF37 | 15 | -22.6 | 0.1 | 6 | 1 | | | | |
| JF37 | 16 | -22.7 | 0.1 | 3 | 0 | | | | |
| JF37 | 17 | -22.8 | 0.1 | 6 | 1 | | | | |
| JF37 | 18 | -22.7 | 0.1 | 13 | 1 | | | | |
| JF37 | 19 | -23.0 | 0.1 | 5 | 0 | | | | |
| JF37 | 20 | -20.7 | 0.1 | 47 | 5 | | | | |
| JF37 | 21 | -19.6 | 0.1 | 6 | 1 | | | | |
| JF37 | 22 | -22.2 | 0.1 | 31 | 3 | | | | |
| Transect 1 | | | | | | | | | |
| JF39 | 10 | -18.2 | 0.1 | 125 | 13 | 6.8 | 1.7 | 330 | 33 |
| JF39 | 9 | -18.6 | 0.1 | 52 | 5 | | | | |
| JF39 | 8 | -18.6 | 0.1 | 43 | 5 | | | | |
| JF39 | 7 | -18.8 | 0.1 | 66 | 7 | | | | |
| JF39 | 6 | -18.5 | 0.2 | 32 | 3 | | | | |
| JF39 | 5 | -18.3 | 0.1 | 16 | 2 | | | | |
| JF39 | 4 | -18.4 | 0.1 | 18 | 2 | | | | |
| JF39 | 3 | -18.4 | 0.1 | 17 | 2 | | | | |
| JF39 | 2 | -16.4 | 0.1 | 4 | 0 | | | | |
| JF39 | 1 | -18.8 | 0.1 | 52 | 5 | | | | |
| | | | | Transect 2 | | | | | |
| JF39 | 16 | -18.8 | 0.1 | | | | | | |
| JF39 | 11 | -18.7 | 0.1 | 17 | 2 | | | | |
| JF39 | 12 | -18.6 | 0.1 | 14 | 1 | | | | |
| JF39 | 13 | -18.5 | 0.1 | 13 | 1 | | | | |
| JF39 | 14 | -18.4 | 0.1 | 20 | 2 | | | | |
| JF39 | 5 | -18.3 | 0.1 | 16 | 2 | | | | |
| JF39 | 15 | -18.3 | 0.1 | 13 | 1 | | | | |
| | | | | Transect 3 | | | | | |
| JF39 | 20 | -18.7 | 0.1 | 43 | 5 | | | | |
| JF39 | 19 | -18.6 | 0.1 | 39 | 4 | | | | |
| JF39 | 8 | -18.6 | 0.1 | 43 | 5 | | | | |
| JF39 | 18 | -18.5 | 0.1 | 44 | 5 | | | | |
| JF39 | 17 | -18.5 | 0.1 | 62 | 6 | | | | |
| | | | | Others | | | | | |
| JF39 | 23 | -16.5 | 0.1 | 4 | 0 | | | | |
| JF39 | 21 | -17.8 | 0.1 | 308 | 33 | 7.1 | 1.6 | 300 | 30 |
| JF39 | 22 | -19.0 | 0.1 | 55 | 6 | | | | |
| | | | | Transect 1 | | | | | |
| JF42 | 11 | -15.9 | 0.2 | 23 | 2 | | | | |
| JF42 | 10 | -16.9 | 0.1 | 49 | 5 | | | | |

| | | | | | |
|---|---|---|---|---|---|
| JF42 | 9 | -17.1 | 0.1 | 18 | 2 |
| JF42 | 8 | -17.4 | 0.1 | 3 | 0 |
| JF42 | 7 | -16.8 | 0.1 | 52 | 5 |
| JF42 | 6 | -17.3 | 0.1 | 4 | 0 |
| JF42 | 5 | -17.4 | 0.1 | 4 | 0 |
| JF42 | 4 | -17.5 | 0.1 | 7 | 1 |
| JF42 | 3 | -17.3 | 0.1 | 3 | 0 |
| JF42 | 2 | -17.4 | 0.1 | 3 | 0 |
| JF42 | 1 | -17.5 | 0.1 | 11 | 1 |
| | | | | Transect 2 | |
| JF42 | 12 | -17.4 | 0.1 | 8 | 1 |
| JF42 | 13 | -17.3 | 0.1 | 6 | 1 |
| JF42 | 5 | -17.4 | 0.1 | 4 | 0 |
| JF42 | 14 | -17.4 | 0.1 | 7 | 1 |
| JF42 | 15 | -17.3 | 0.1 | 8 | 1 |
| | | | | Others | |
| JF42 | 19 | -21.8 | 0.1 | 58 | 6 |
| JF42 | 16 | -16.6 | 0.1 | 51 | 5 |
| JF42 | 20 | -21.8 | 0.1 | 54 | 5 |
| JF42 | 17 | -17.2 | 0.1 | 3 | 0 |
| JF42 | 18 | -16.4 | 0.1 | 21 | 2 |
| | | | | Transect 1 | |
| JF43 | 6 | -21.2 | 0.1 | 23 | 2 |
| JF43 | 5 | -21.6 | 0.1 | 4 | 0 |
| JF43 | 4 | -21.5 | 0.1 | 3 | 0 |
| JF43 | 3 | -17.3 | 0.1 | 1 | 0 |
| JF43 | 2 | -17.1 | 0.1 | 1 | 0 |
| JF43 | 1 | -17.4 | 0.1 | 2 | 0 |
| | | | | Transect 2 | |
| JF43 | 7 | -17.2 | 0.1 | 2 | 3 |
| JF43 | 8 | -17.1 | 0.1 | 2 | 3 |
| JF43 | 2 | -17.1 | 0.1 | 1 | 1 |
| JF43 | 9 | -17.2 | 0.1 | 2 | 1 |
| JF43 | 10 | -17.1 | 0.1 | 2 | 5 |
| JF43 | 11 | -17.2 | 0.1 | 2 | 5 |
| | | | | Others | |
| JF43 | 15 | -21.7 | 0.1 | 31 | 2 |
| JF43 | 14 | -20.8 | 0.1 | 2 | |
| JF43 | 13 | -21.4 | 0.1 | 12 | 6 |
| JF43 | 12 | -21.5 | 0.1 | 3 | 1 |
| | | | | Transect 1 | |
| JF44 | 1 | -17.8 | 0.1 | 1 | 0 |
| JF44 | 2 | -17.7 | 0.1 | 3 | 0 |
| JF44 | 3 | -17.8 | 0.1 | 2 | 0 |
| JF44 | 4 | -17.6 | 0.1 | 2 | 0 |
| JF44 | 5 | -18.1 | 0.1 | 2 | 0 |
| JF44 | 6 | -17.7 | 0.1 | 1 | 0 |
| JF44 | 7 | -17.9 | 0.1 | 5 | 1 |
| JF44 | 8 | -18.0 | 0.1 | 7 | 1 |
| JF44 | 16 | -18.0 | 0.1 | 9 | 1 |
| JF44 | 9 | -18.2 | 0.1 | 10 | 1 |
| JF44 | 10 | -18.3 | 0.1 | 9 | 1 |
| JF44 | 11 | -18.3 | 0.2 | 9 | 1 |
| | | | | Transect 2 | |
| JF44 | 14 | -18.3 | 0.1 | 9 | 1 |
| JF44 | 15 | -18.1 | 0.1 | 8 | 1 |
| JF44 | 16 | -18.0 | 0.1 | 9 | 1 |
| JF44 | 17 | -18.3 | 0.1 | 6 | 1 |

| | | | | | | | | | |
|---|---|---|---|---|---|---|---|---|---|
| JF44 | 18 | -18.2 | 0.1 | 8 | 1 | | | | |
| | | | | Others | | | | | |
| JF44 | 12 | -18.3 | 0.1 | 4 | 0 | | | | |
| JF44 | 13 | -18.4 | 0.2 | 22 | 3 | | | | |
| | | | | Transect 1 | | | | | |
| JF50 | 1 | -23.2 | 0.1 | 152 | 16 | -0.2 | 2.2 | 149 | 15 |
| JF50 | 2 | -22.7 | 0.1 | 69 | 8 | | | | |
| JF50 | 3 | -22.9 | 0.1 | 65 | 8 | | | | |
| JF50 | 4 | -22.8 | 0.1 | 83 | 9 | 1.1 | 3.1 | 82 | 8 |
| JF50 | 5 | -23.3 | 0.1 | 135 | 15 | 0.3 | 2.6 | 105 | 10 |
| JF50 | 6 | -22.4 | 0.1 | 24 | 2 | | | | |
| JF50 | 7 | -20.9 | 0.1 | 4 | 0 | | | | |
| JF50 | 8 | -20.3 | 0.1 | 2 | 0 | | | | |
| | | | | Transect 2 | | | | | |
| JF50 | 15 | -22.4 | 0.1 | 20 | 2 | | | | |
| JF50 | 14 | -22.4 | 0.1 | 9 | 1 | | | | |
| JF50 | 13 | -22.7 | 0.1 | | | | | | |
| JF50 | 12 | -22.8 | 0.1 | 88 | 10 | -0.8 | 2.8 | 91 | 9 |
| JF50 | 11 | -22.5 | 0.1 | 62 | 7 | | | | |
| JF50 | 3 | -22.7 | 0.1 | 69 | 8 | | | | |
| JF50 | 10 | -22.6 | 0.1 | 59 | 6 | | | | |
| JF50 | 9 | -22.9 | 0.1 | 68 | 7 | | | | |
| | | | | Others | | | | | |
| JF50 | 16 | -22.5 | 0.1 | 12 | 1 | | | | |
| JF50 | 17 | -20.5 | 0.1 | 2 | 0 | | | | |
| | | | | Transect 1 | | | | | |
| JF55 | 1 | -18.0 | 0.2 | 8 | 1 | | | | |
| JF55 | 2 | -17.7 | 0.1 | 3 | 0 | | | | |
| JF55 | 3 | -18.7 | 0.1 | 5 | 1 | | | | |
| JF55 | 4 | -18.1 | 0.1 | 3 | 0 | | | | |
| JF55 | 5 | -17.8 | 0.1 | 6 | 1 | | | | |
| JF55 | 8 | -17.7 | 0.1 | 5 | 1 | | | | |
| | | | | Transect 2 | | | | | |
| JF55 | 11 | -17.9 | 0.1 | 11 | 1 | | | | |
| JF55 | 12 | -18.0 | 0.1 | 32 | 3 | | | | |
| JF55 | 5 | -17.8 | 0.1 | 6 | 1 | | | | |
| JF55 | 13 | -17.8 | 0.1 | 10 | 1 | | | | |
| JF55 | 14 | -18.6 | 0.1 | 6 | 1 | | | | |
| | | | | Others | | | | | |
| JF55 | 6 | -17.8 | 0.1 | 19 | 2 | | | | |
| JF55 | 7 | -17.7 | 0.1 | 3 | 0 | | | | |
| JF55 | 9 | -17.9 | 0.1 | 3 | 0 | | | | |
| JF55 | 10 | -17.9 | 0.2 | 37 | 4 | | | | |
| JF55 | 15 | -17.8 | 0.1 | 238 | 25 | 7.1 | 1.6 | 300 | 30 |
| JF55 | 16 | -17.8 | 0.1 | | | | | | |
| JF55 | 17 | -18.0 | 0.1 | 29 | 3 | | | | |
| | | | | Transect 1 | | | | | |
| JF58 | 1 | -21.6 | 0.1 | 74 | 8 | | | | |
| JF58 | 2 | -20.5 | 0.1 | 53 | 5 | | | | |
| JF58 | 3 | -16.0 | 0.3 | 47 | 5 | | | | |
| JF58 | 4 | -19.3 | 0.1 | 44 | 5 | | | | |
| JF58 | 5 | -19.4 | 0.1 | 46 | 5 | | | | |
| JF58 | 6 | -19.3 | 0.1 | 41 | 4 | | | | |
| JF58 | 7 | -19.8 | 0.1 | 49 | 5 | | | | |
| JF58 | 8 | -20.3 | 0.1 | 61 | 7 | | | | |
| | | | | Others | | | | | |
| JF58 | 9 | -21.8 | 0.1 | 77 | 8 | | | | |
| JF58 | 10 | -19.3 | 0.1 | 49 | 5 | | | | |

| | | | | | |
|---|---|---|---|---|---|
| JF58 | 11 | -19.3 | 0.1 | 54 | 6 |
| JF58 | 12 | -19.5 | 0.1 | 51 | 6 |

[a] Measured with carbon isotopic analyses.
[b] Measured with nitrogen isotopic analyses.

Table 4 Output parameters of the Rayleigh fractionation modelling of the Monastery and Jagersfontein diamonds. ΔC and ΔN = isotopic fractionation factor of carbon and nitrogen between diamond and diamond forming-fluid, $K_N$ = nitrogen partition coefficient between diamond and the fluid, $\delta^{13}C_0$ and $\delta^{15}N_0$= initial carbon and nitrogen isotopic composition of the fluid and $N_0$= initial nitrogen content of the fluid. Temperatures are estimates based on majorite inclusion barometry (see Fig. 1) projected on the mantle adiabat of Katsura et al. (2010).

| Diamond | Temperature (°C) | ΔC | $K_N$ | $\delta^{13}C_o$ | $\delta^{15}N_o$ | $N_o$ | ΔN |
|---|---|---|---|---|---|---|---|
| | | | | Oxidized fluids | | | |
| **Mon B9-07** | 1550 | -1.0 | 6.0 | -14.7 | 6.8 | 420 | -3.0 |
| **JF09** | 1480 | -2.5 | 7.0 | -20.7 | | 5 | |
| **JF44** | 1520 | -2.0 | 10.0 | -16.4 | | 2 | |
| **JF50** | 1480 | -2.8 | 6.5 | -20.5 | | 24 | |
| | | | | Reduced fluids | | | |
| **Mon A4-03** | 1550 | 1.2 | 0.3 | -15.5 | | 27 | |
| **JF58** | 1490 | 1.5 | 0.7 | -20.7 | | 65 | |

**Supplementary material**

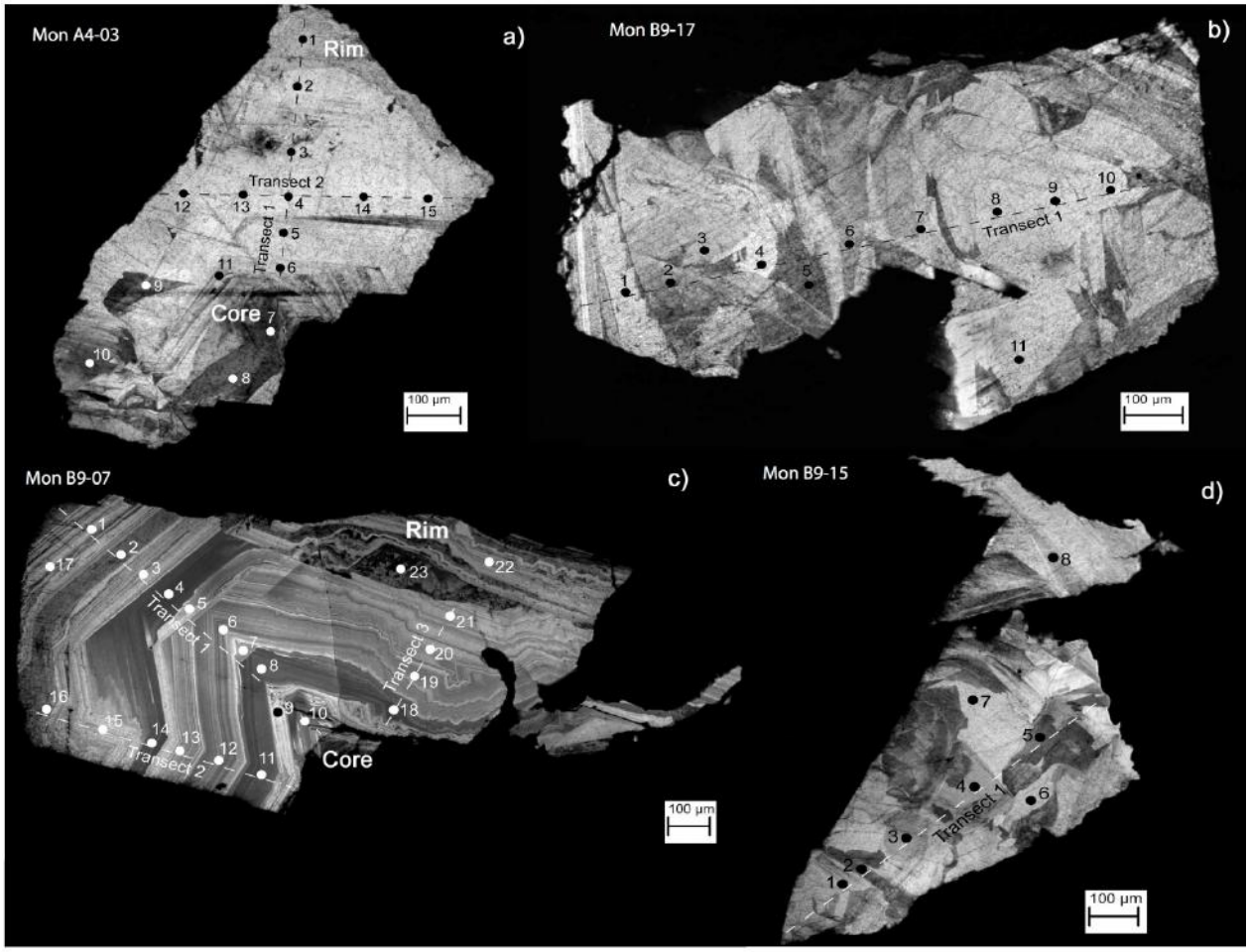


Appendix A: Cathodoluminescence images of all the studied Monastery diamonds. Transects are indicated on the CL images.

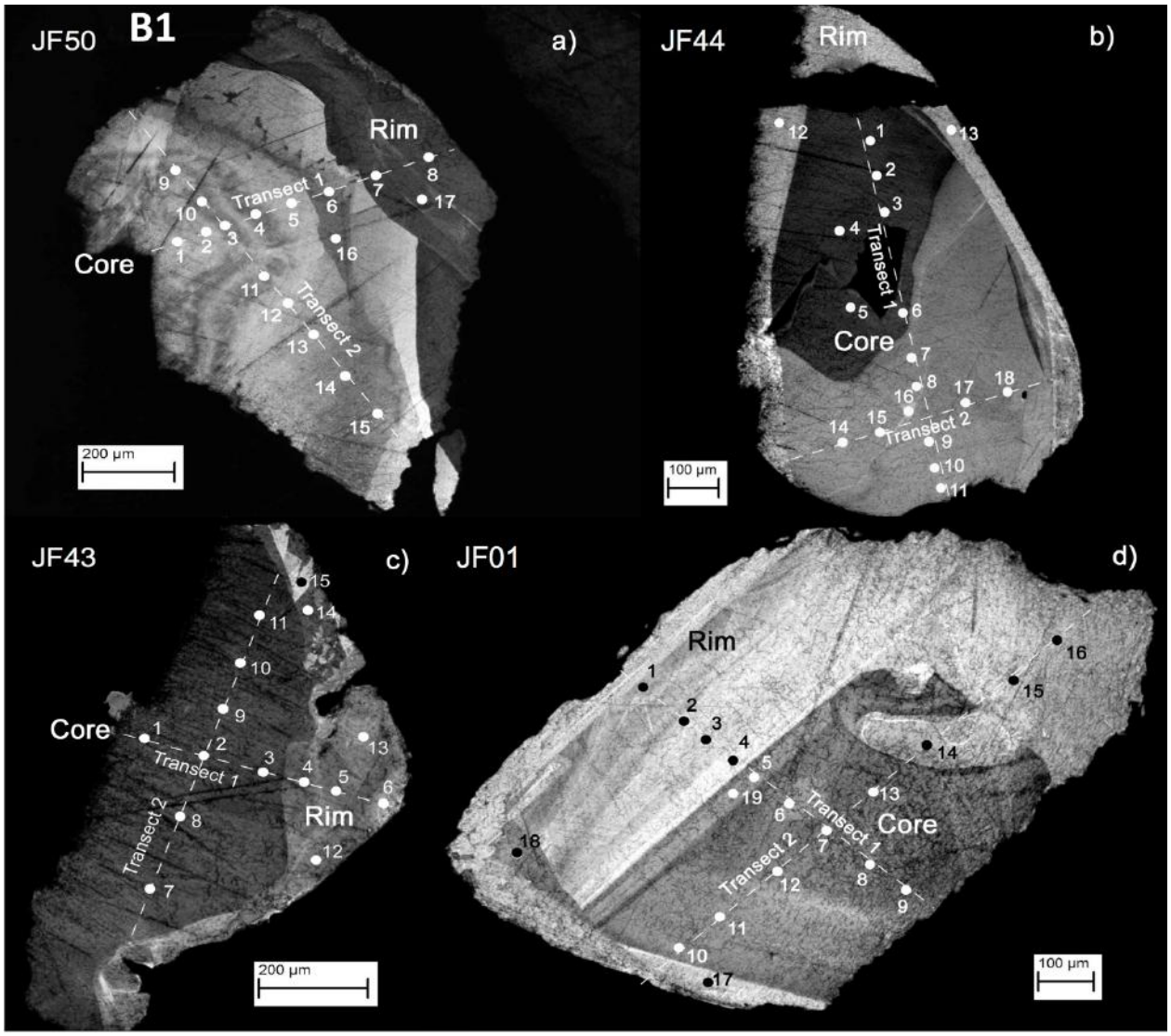


Appendix B1: Cathodoluminescence images of Jagersfontein diamonds. Transects are indicated on the CL images.

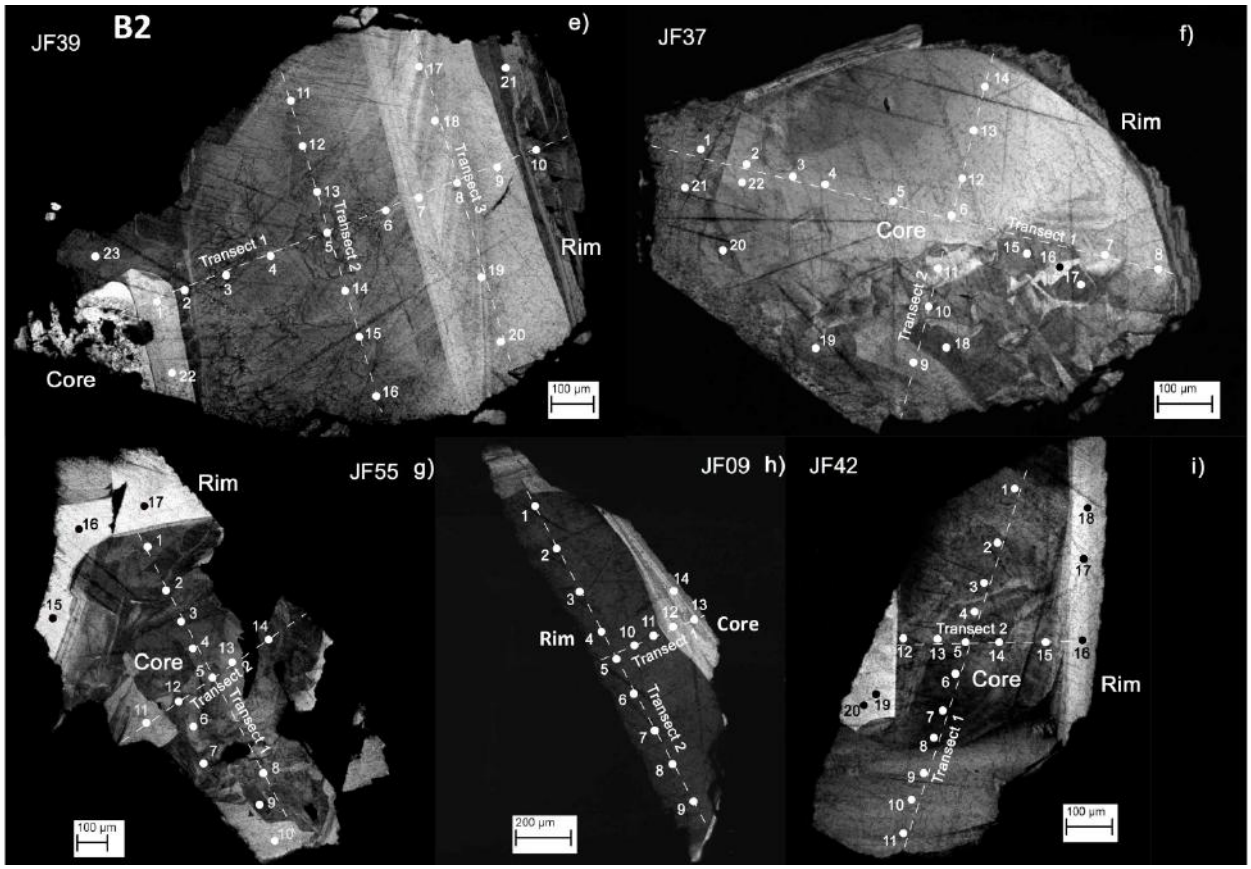


Appendix B2: Cathodoluminescence images of Jagersfontein diamonds. Transects are indicated on the CL images.

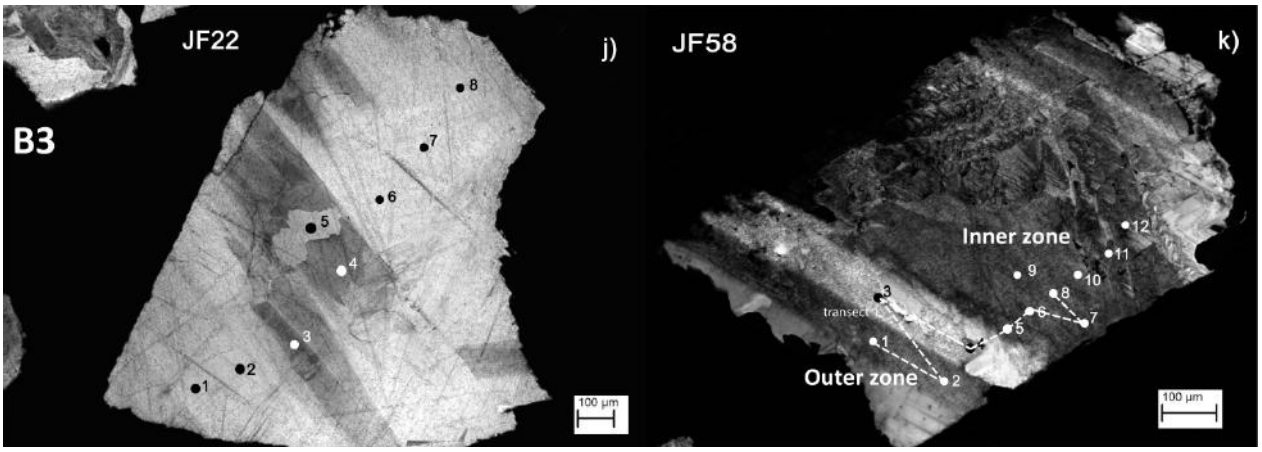


Appendix B3: Cathodoluminescence images of Jagersfontein diamonds. Transects are indicated on the CL images.

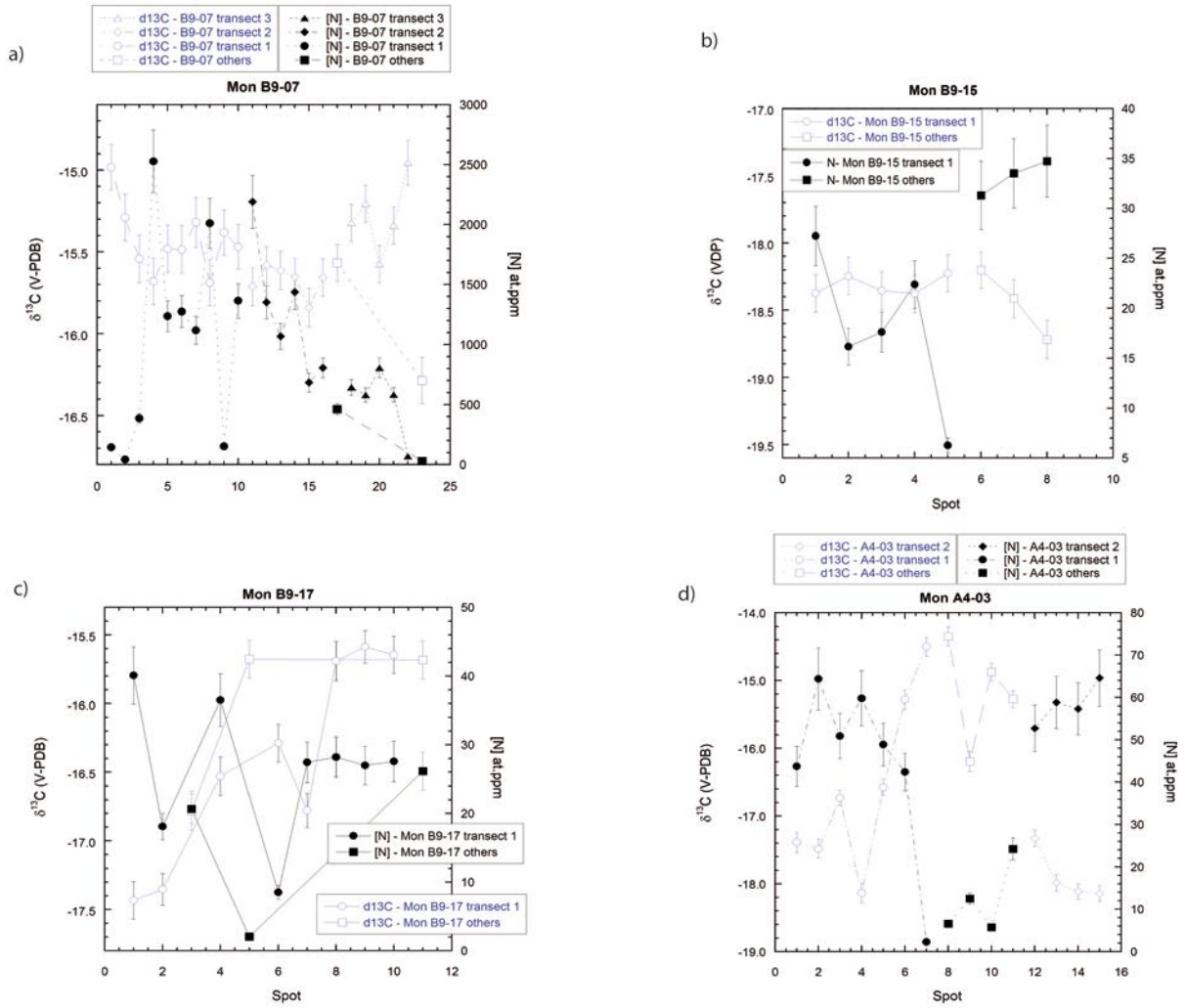


Appendix C: $\delta^{13}C$ -N-spot profiles of the Monastery diamonds. Error bars are 2 σ.

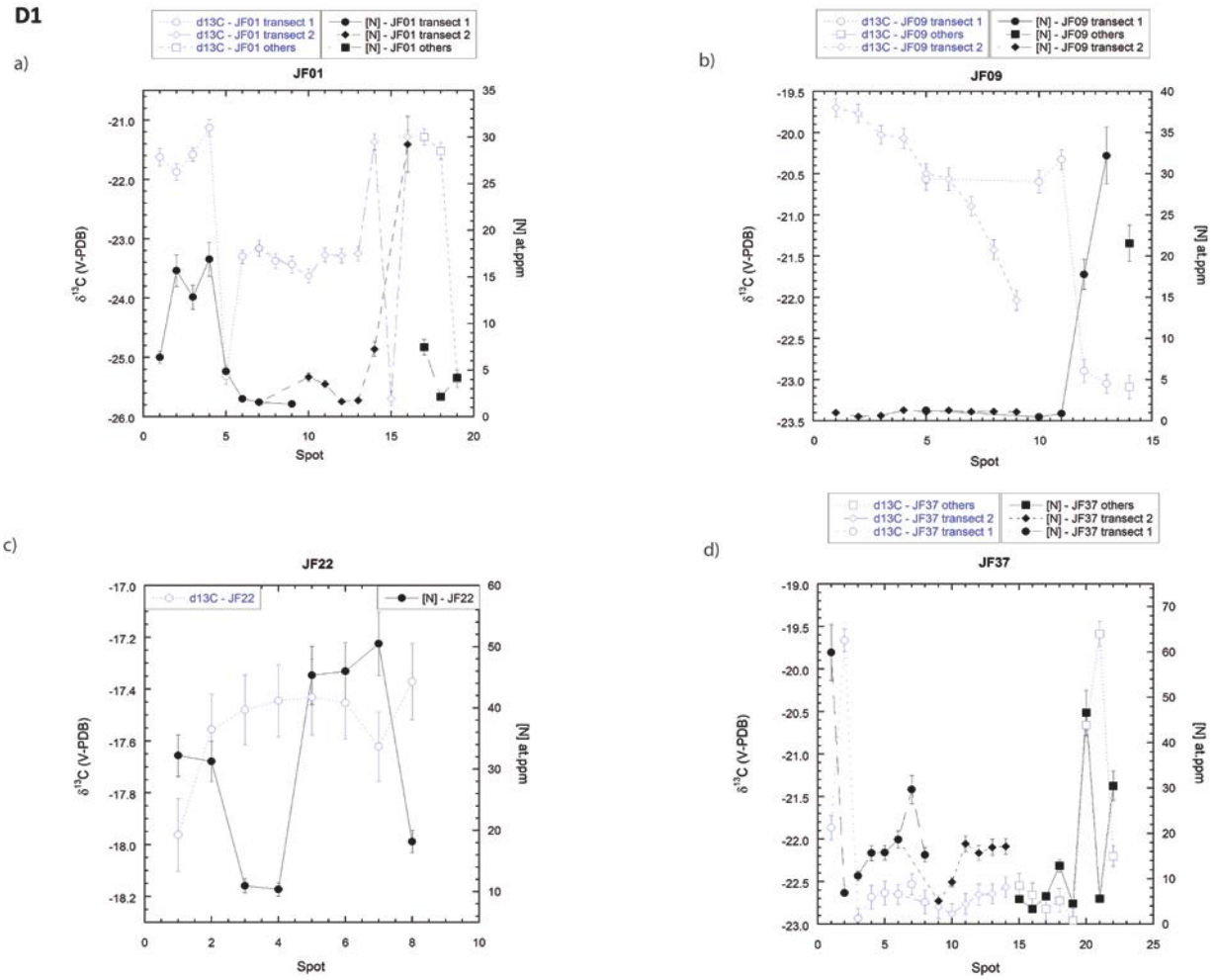


Appendix D1: $\delta^{13}C$ -N-spot profiles of the Jagersfontein diamonds. Error bars are 2 σ.

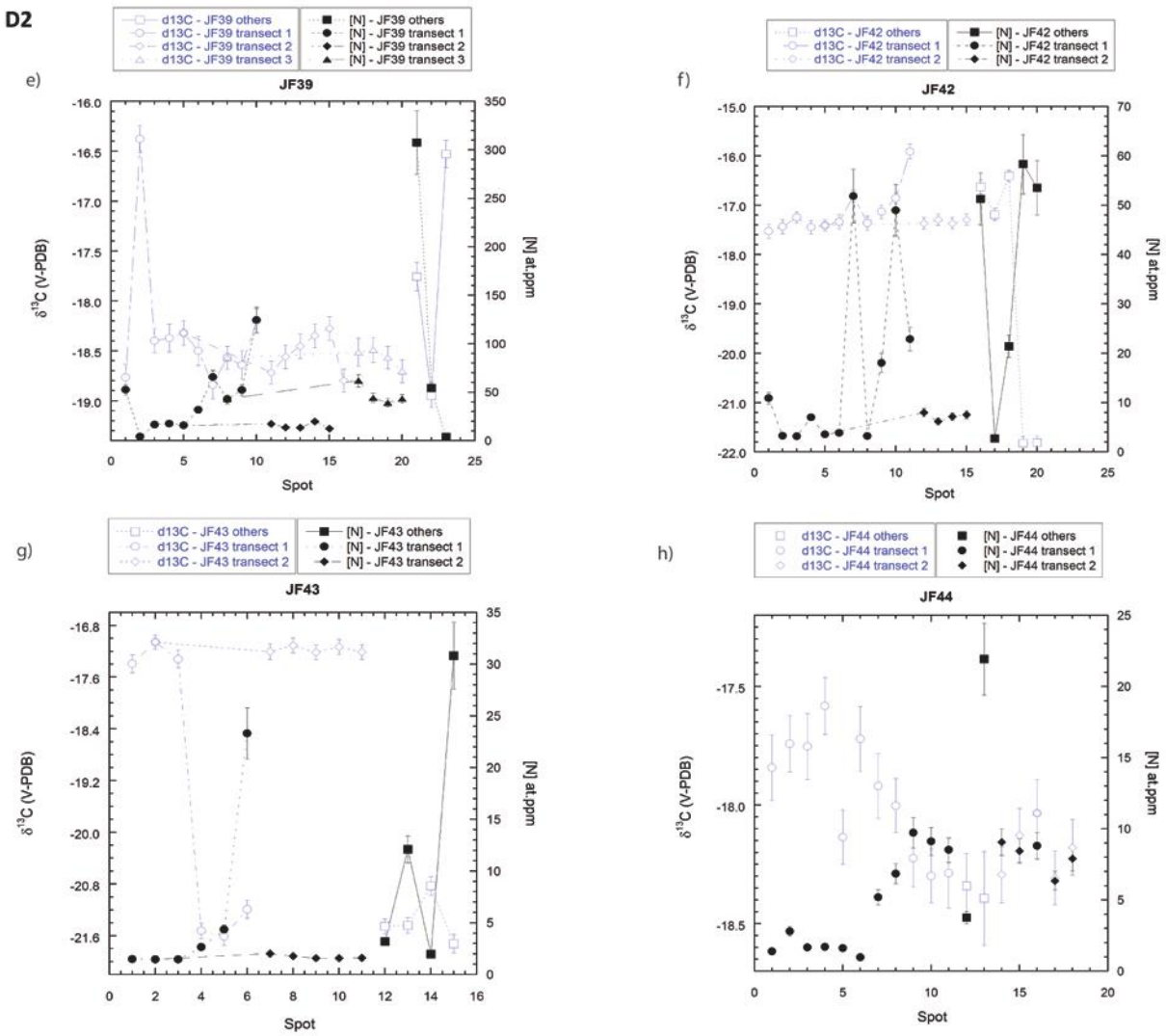


Appendix D2: $\delta^{13}C$ -N-spot profiles of the Jagersfontein diamonds. Error bars are 2 σ.

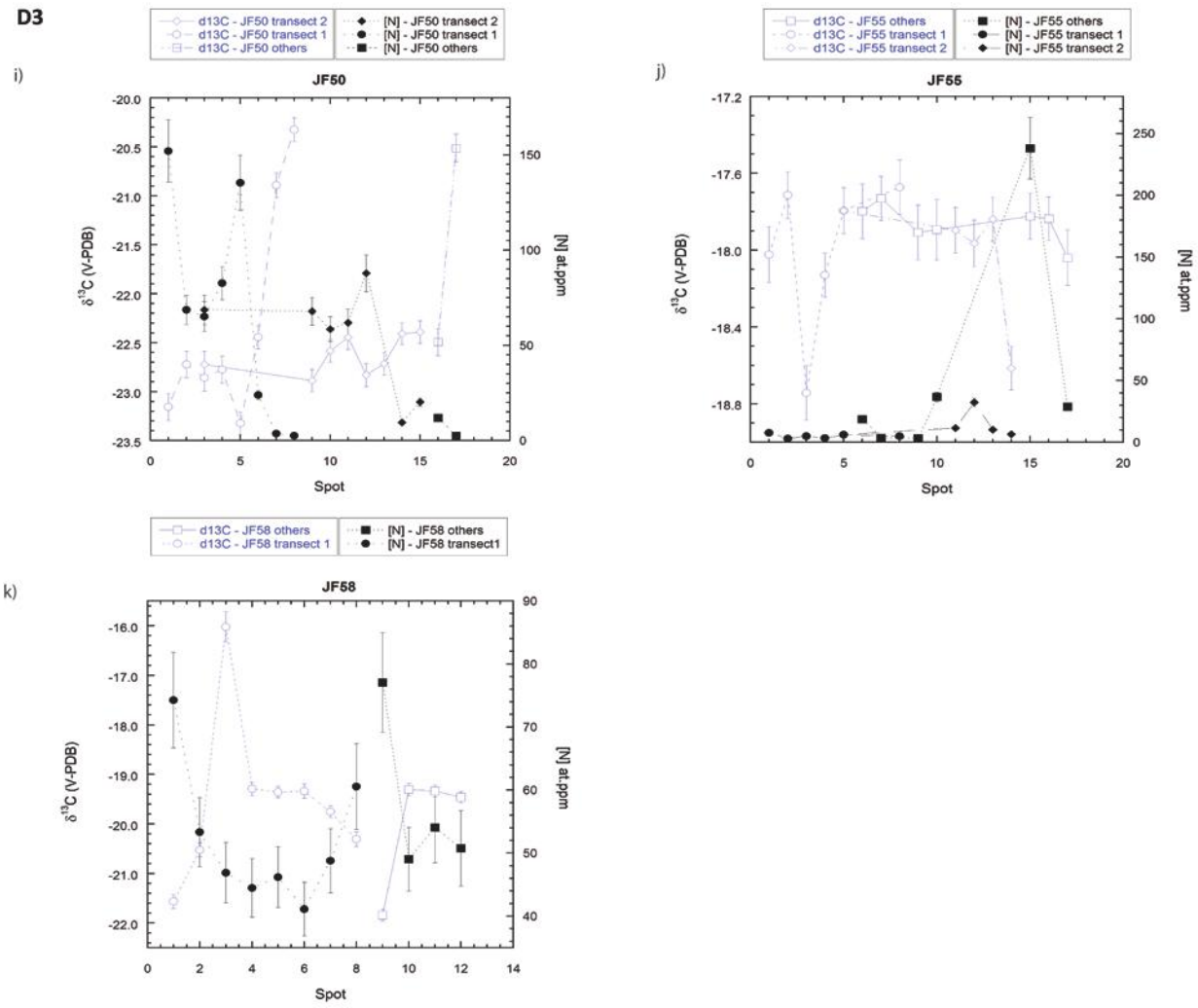


Appendix D3: $\delta^{13}C$ -N-spot profiles of the Jagersfontein diamonds. Error bars are 2 σ.

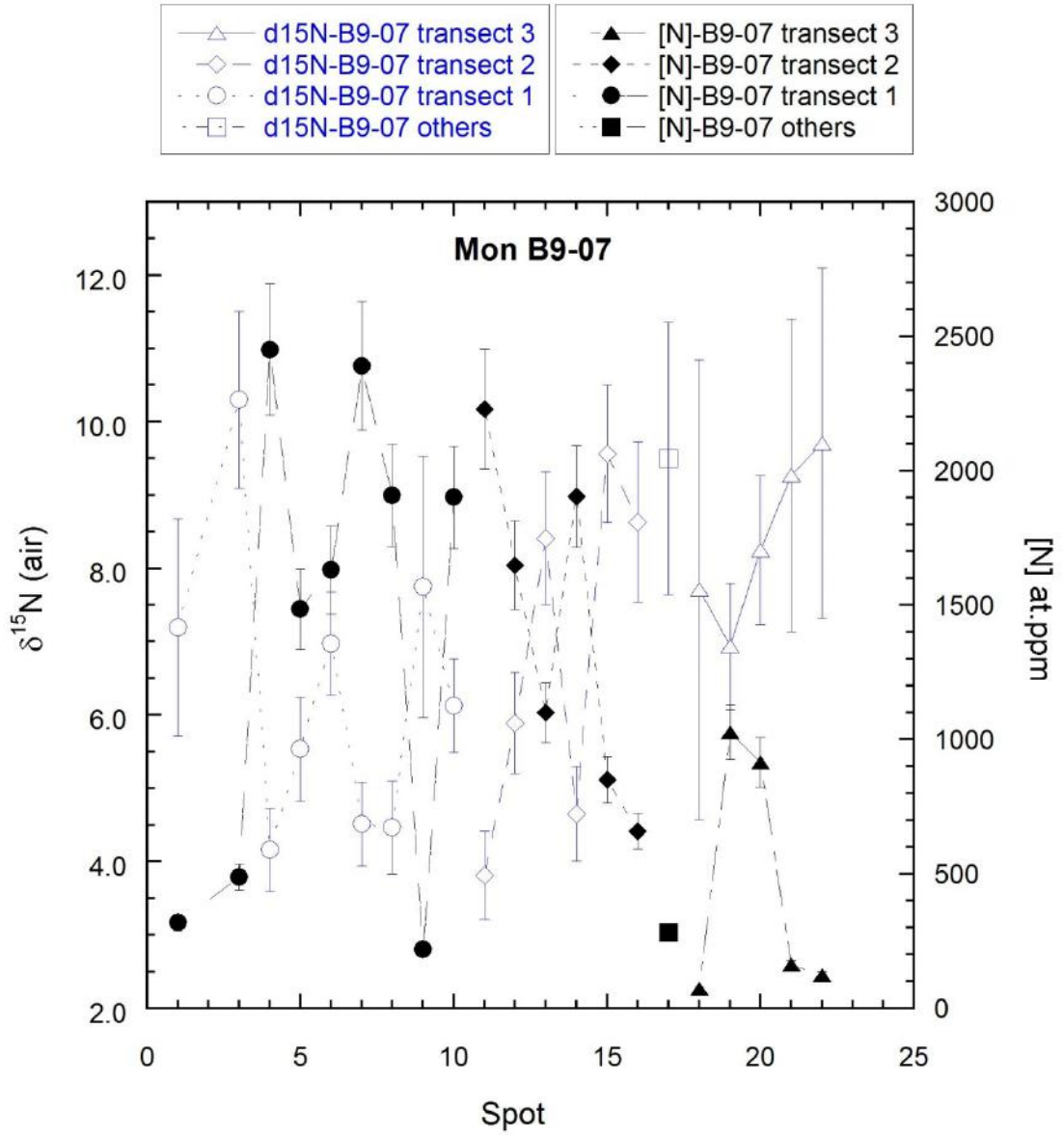


Appendix E: $\delta^{15}N$ -N-spot profiles of Mon B9-07 diamond. Error bars are 2 σ.